frontiers in
CELLULAR NEUROSCIENCE

TECHNOLOGY REPORT ARTICLE
published: 07 October 2013
doi: 10.3389/fncel.2013.00175

Comparative neuronal differentiation of self-renewing neural progenitor cell lines obtained from human induced pluripotent stem cells

Chiara Verpelli[1], Luigi Carlessi[2], Giulia Bechi[3], Elena Fusar Poli[2], Daniel Orellana[4], Christopher Heise[1], Silvana Franceschetti[3], Renato Mantegazza[4], Massimo Mantegazza[3,5], Domenico Delia[2] and Carlo Sala[1,4]**

[1] CNR Institute of Neuroscience and Department of Biotechnology and Translational Medicine, University of Milan, Milan, Italy
[2] Department of Experimental Oncology, Fondazione IRCCS Istituto Nazionale dei Tumori, Milan, Italy
[3] Department of Neurophysiopathology, Foundation Carlo Besta Neurological Institute, Milan, Italy
[4] Neuromuscular Diseases and Neuroimmunology, Foundation Carlo Besta Neurological Institute, Milan, Italy
[5] Institute of Molecular and Cellular Pharmacology, LabEx ICST, CNRS UMR7275 and University of Nice-Sophia Antipolis, Valbonne, France

Edited by:
Eran Meshorer, The Hebrew University of Jerusalem, Israel

Reviewed by:
Dorit Cohen-Carmon, Hebrew University of Jerusalem, Israel

***Correspondence:**
Chiara Verpelli and Carlo Sala, CNR Institute of Neuroscience, Via Vanvitelli 32, 20129 Milano, Italy
e-mail: c.verpelli@in.cnr.it; c.sala@in.cnr.it

Most human neuronal disorders are associated with genetic alterations that cause defects in neuronal development and induce precocious neurodegeneration. In order to fully characterize the molecular mechanisms underlying the onset of these devastating diseases, it is important to establish *in vitro* models able to recapitulate the human pathology as closely as possible. Here we compared three different differentiation protocols for obtaining functional neurons from human induced pluripotent stem cells (hiPSCs): human neural progenitors (hNPs) obtained from hiPSCs were differentiated by co-culturing them with rat primary neurons, glial cells or simply by culturing them on matrigel in neuronal differentiation medium, and the differentiation level was compared using immunofluorescence, biochemical and electrophysiological methods. We show that the differentiated neurons displayed distinct maturation properties depending on the protocol used and the faster morphological and functional maturation was obtained when hNPs were co-cultured with rat primary neurons.

Keywords: induced pluripotent stem cells, neuronal differentiation, synapse formation, Human neurons, postsynapse

INTRODUCTION

Neuronal disorders in humans can be caused by defects in neuronal development and neurodegenerative processes, and are often related to functional alterations of cortical neurons (Calahorro and Ruiz-Rubio, 2011; Penzes et al., 2011; Esposito et al., 2012; Marcello et al., 2012; Verpelli and Sala, 2012). In order to fully characterize the molecular mechanisms underlying the onset of these diseases, it is important to establish new *in vitro* models able to recapitulate the human pathology as closely as possible.

The recently developed techniques which allow the neural differentiation of skin fibroblast-derived human induced pluripotent stem cells (hiPSCs) represent an innovative strategy to study neuronal development and degeneration, circuit formation and function, and for generating new *in vitro* human models of brain diseases (Takahashi and Yamanaka, 2006; Dimos et al., 2008; Wernig et al., 2008; Marchetto et al., 2010; Xu et al., 2010; Ricciardi et al., 2012; Yamanaka, 2012; Carlessi et al., 2013a). For this reason, it is crucial to define a reproducible method for obtaining wild type and disease-derived mature neurons which can be employed for functional and comparative analysis. Previous works have described several methods to obtain self-renewing neural progenitors (hNPs) from embryonic stem cells (ESCs) (Reubinoff et al., 2001; Zhang et al., 2001; Peng and Chen, 2005; Axell et al., 2009) and from hiPSCs (Wernig et al., 2008; Shi et al., 2012; Carlessi et al., 2013b), which can then be successfully differentiated into patient-derived neurons (Marchetto et al., 2010; Zhang et al., 2010; Pasca et al., 2011; Aboud et al., 2012; D'aiuto et al., 2012; Farra et al., 2012; Israel et al., 2012; Paulsen et al., 2012; Xia et al., 2012; Yin et al., 2012; Salewski et al., 2013). As various protocols have been employed for this purpose, a comparative study describing the timing and level of differentiation achieved with different methodologies could help decide the best suitable approach to obtain neurons to be used as *in vitro* models of neurological diseases.

Here we followed a reproducible technique for obtaining hNPs from hiPSCs, which we then differentiated into neurons applying three different protocols: co-culture with rat primary neurons or glial cells or culture on matrigel, showing that they display distinct differentiation properties depending on the protocol used.

MATERIALS AND METHODS

CELL CULTURE AND hiPSC GENERATION

Fibroblasts were obtained from skin biopsies of three healthy donors (called D1-3) under the approval of the Ethics Board. Cells were maintained and expanded in Dulbecco's modified Eagle medium supplemented with 20% fetal bovine serum and penicillin/streptomycin (P/S) (all from *Invitrogen*). Fibroblasts were

infected with STEMCCA Cre-Excisable Constitutive Polycistronic Lentivirus (Millipore) following the manufacturer's instructions. After 25 days, hiPSC clones were manually picked and directly transferred on mitomycin C-treated mouse embryonic fibroblasts in human ESC medium composed of DMEM/F12 containing 20% KSR (vol/vol), 10 ng ml^{-1} bFGF, 1 mM glutamine, 100 μm non-essential amino acids, 100 μM 2-mercaptoethanol, 50 U ml^{-1} penicillin and 50 mg ml^{-1} streptomycin (all from *Invitrogen*).

GENERATION OF NEURAL PROGENITOR CELLS

At least one clone for each donor was processed for neural differentiation, but the results of the experiments were obtained with clones #1 of donors 1 and 2 (D1 and D2), and both clones produced exactly the same results.

hiPSC lines were detached with Collagenase IV and resuspended in human ESC medium without bFGF to form embryoid bodies (EBs), which were cultured in suspension in low adhesion non-treated sterile dishes (Nunc). After 5 days, EBs were collected and plated in matrigel-coated dishes and grown for additional 4 days in 1X N2 media supplemented with 20 ng/ml bFGF in order to obtain neural rosettes. Rosettes were then manually picked, resuspended to single cells in NP medium, composed of DMEM/F12 containing 2 mM glutamax, B27 1:500, N2 1:100, 1% P/S, 20 ng/ml EGF, 20 ng/ml bFGF, and plated in matrigel-coated flasks. NP medium was changed every 2 days; once the cell culture reached 95% confluence, cells were dissociated with Accutase (*Invitrogen*). After dissociation with Accutase 1×10^7 cells were blocked in 1% BSA in PBS and incubated with 20 μL of anti-PSA-NCAM antibody conjugated with magnetic micro-beads (Cat. No. 130-092-966, Miltenyi Biotec) for 15 min at 4°C. After washing, the cell suspension was loaded on the separation column and collected through the magnet provided by the Miltenyi Biotec company. Negatively-labeled cells which passed through during column-washing were discarded, whereas positively-labeled cells that remained in the column were eluted to another tube with culture media after removing the column from the magnetic stand. These were further cultured and expanded up to 30 passages (Kim et al., 2012).

TERMINAL DIFFERENTIATION OF hNPs AND LENTIVAIRAL INFECTION

hNPs were differentiated following different protocols and the experiments were repeated on two lines of hNPs (obtained from hiPSC clone #1 of D1 and hiPSC clone #1 of D2) at the same passages (at passage 5 or 6). For differentiation on rat cortical neuronal cells, primary rat cultures were extracted from 18- to 19-day-old rat embryos (pregnant female rats were obtained from Charles River Laboratories). The neurons were plated at medium density (150–200 cells/mm^2) and grown as described in Verpelli et al. (2010); at DIV 7, 20,000 hNPs infected with Syn:EGFP were plated onto the cortical neurons; medium was changed every 4 days until day 88.

For differentiation on glial cells, rat glia was prepared as described in Goslin and Banker (1991) and 20,000 hNPs were plated onto 75,000 glial cells. Two days after plating, glial medium was replaced with Neurobasal medium supplemented with B27 (*Invitrogen*); medium was changed every 4 days until day 63.

For differentiation with medium, 4000 hNPs were detached and plated on matrigel-coated coverslips in NP medium without bFGF and EGF. Medium was changed every 4 days until day 63.

IMMUNOCYTOCHEMISTRY

Cells were fixed in 4% paraformaldehyde and 4% sucrose at room temperature or in 100% methanol at −20°C. Primary and secondary antibodies were applied in GDB buffer composed of 30 mM phosphate buffer, pH 7.4, containing 0.2% gelatin, 0.5% Triton X-100, and 0.8 mM NaCl. Primary antibodies were applied for 3 h at room temperature or overnight at 4°C. Secondary antibodies were applied for 1 h at room temperature.

Confocal images of 1024 × 1024 pixels were obtained with a LSM 510 Meta confocal microscope (Carl Zeiss, a gift from Fondazione Monzino) and a 63× objective with sequential acquisition settings. Each image was a Z-series projection of 7–15 images, each averaged 2–4 times, and taken at 0.4–0.7-μm depth intervals.

ANTIBODIES

The following antibodies were used: rabbit anti-NANOG (Abcam), mouse anti-OCT3\4 (Santa Cruz Biotechnology), mouse anti-TRA-1-81 (eBioscience), mouse anti-SSEA4 (eBioscience), mouse anti-βTubulin III (Sigma), mouse anti-SOX17 (R&D), mouse aSMA (Sigma), mouse anti-vinculin (Sigma), mouse anti-Nestin (Chemicon), mouse anti-Neuronal Nuclei (Millipore), mouse anti-MAP2 (Abcam), mouse anti-Human Nuclei (Millipore), rabbit anti-VGLUT (Synaptic System), mouse anti-synaptophysin (Sigma), mouse and rabbit anti-GFAP (Sigma), mouse anti-PSD-95 (NeuroMab, University of California, Davis/NIH NeuroMab Facility); rabbit anti-VGAT (Synaptic System), mouse anti-SCG10 (NeuroMab), mouse anti-Pan-KChIP (NeuroMab), rabbit anti-GABA (Sigma) and mouse anti-GAD67 (Millipore), rabbit anti-PAX6 (Covance), rabbit anti-Ki67 (Thermo Scientific), mouse anti-Sox2 (Abcam); secondary FITC-, Cy3- and Cy5-conjugated anti-mouse and anti-rabbit (Jackson ImmunoResearch); secondary HRP-conjugated anti-mouse and anti-rabbit (GE Healthcare).

ELECTROPHYSIOLOGICAL RECORDINGS AND ANALYSIS

When plated on primary cortical neurons or on primary glial cells, hNP-derived neurons were selected by their fluorescence. Recordings were done at room temperature (22–25°C) using a Multiclamp 700A patch-clamp amplifier and pClamp 10.2 software (Molecular Devices) as in Cestèle et al. (2008). For the recordings of total ionic currents, signals were filtered at 10 kHz and sampled at 100 kHz. We recorded sodium currents using the whole-cell configuration of the patch-clamp technique. Recordings were usually started 5 min after the rupture of the membrane patch, to allow intracellular dialysis with the pipette solution. The external bath solution contained the following (in mM): 129 NaCl, 1.25 NaH_2PO_4, 35 glucose, 1.8 $MgSO_2$, 1.6 $CaCl_2$, 3 KCl and 10 HEPES, pH 7.4 with NaOH; the internal pipette solution contained the following (in mM): 120 K-gluconate, 15 KCl, 2 $MgCl_2$, 0.2 EGTA, 10 HEPES, 20 P-creatine, 2 Na_2ATP, 0.2 Na_2GTP and 0.1 Leupeptine, pH 7.2 with KOH. Cell capacitance and series resistance errors were carefully

compensated (∼85%) throughout the experiment. Pipette resistance was between 2.6 and 3.0 MΩ. For the recordings of postsynaptic currents, signals were filtered at 3 kHz and sampled at 10 kHz. We used 3 mM kynurenic acid and 10 μM bicuculline to block glutamatergic and GABAergic postsynaptic currents, respectively. Postsynaptic currents were identified as the events larger than 2 times the RMS noise of the eventless periods in the trace. When we switched to current-clamp mode, we applied the bridge balance compensation and recorded neuronal firing by injecting depolarizing current pulses of increasing amplitude; for these experiments, we held the resting potential at −70 mV by injecting the appropriate holding current, in order to compare the firing of different cells in the same conditions. The neurons with unstable resting potential and/or unstable firing were discarded. In current clamp mode, signals were filtered at 10 kHz and sampled at 20 kHz.

WESTERN BLOTTING

Total cell extracts and Western blot analysis were performed as previously described in Carlessi et al. (2009). Briefly, cells were lysed in Laemmli buffer (0.125 M Tris–HCl pH 6.8, 5% SDS) and lysates were sonicated, size-fractionated by SDS–PAGE and electroblotted onto PVDF membranes (Millipore, Bedford, MA), which were incubated with the indicated primary antibodies. Binding of the antibodies to the membranes was detected using peroxidase-conjugated secondary antibodies and ECL (Pierce, Rockford, IL) on autoradiographic films. Bands were acquired with a digital scanner.

RNA ISOLATION AND PCR ANALYSIS

All RNA samples were extracted with RNeasy Micro Kit (Quiagen) from about 1 to 5×10^6 cells, according to the manufacturer's instructions. RNAs were retro-transcribed using the Transcriptor High Fidelity cDNA Synthesis Kit (Roche) and cDNAs were amplified by Amplibiotherm DNA polymerase (Fisher Molecular Biology). For qRTPCR, we used the STEMCCA Viral Gene Detection qPCR Multiplex Kit (Millipore).

VIRUS CONSTRUCT AND PRODUCTION

Lentiviruses were produced in 293T packaging cells as previously described in Naldini et al. (1996) and Lois et al. (2002).

RESULTS

GENERATION OF hiPSC LINES

We generated hiPSC lines from fibroblasts obtained from three healthy control donors (called D1-3) using the hSTEMCCA-loxP virus (Millipore) as described in the manufacturer's protocol. We obtained at least 10 independent clones from each fibroblast culture. We maintained the colonies, expressing alkaline phosphatase, on mitomycin-inactivated mouse embryonic fibroblasts (MEFs) (**Figure 1A** shows two iPS clones, #1 and #2, from donor 1) and the plurypotency of each clone was confirmed by RT analysis of markers such as OCT4, Nanog and Lin28 (**Figure 1B**, results obtained only from clones #1 of each donor are shown as representative examples). Moreover, all clones also expressed Nanog, Oct 3/4, Tra-1-81 and SSEA4, which were detected by immunofluorescence (**Figure 1C**, clone #1 from donor 1 is shown as a representative example). We analyzed the ability of our hiPSC clones to spontaneously differentiate into the three germ layers in the absence of mitogenic factors by observing the expression of βTubulin III, Sox17, and aSMA as markers of ectoderm, endoderm and mesoderm, respectively (**Figure 1D**, clone #1 from donor 1 is shown as a representative example). Finally, we tested the ability of two independent clones, for each starting fibroblast line (D1-3), to induce teratoma in mice (data not shown) as described in Ricciardi et al. (2012). Interestingly, two of the fibroblast cultures that we reprogrammed were originally infected by mycoplasma and were rescued by extensive use of BM-Cyclin (ROCHE) before infection with hSTEMCA-loxP virus. The hiPSC colonies we obtained were completely free of mycoplasma (**Figures A1A,B**).

GENERATION AND CHARACTERIZATION OF HUMAN SELF-RENEWING NEURAL PROGENITORS (hNPs)

We started neural differentiation by inducing the formation of embryoid bodies (EBs) from hiPSC colonies at passage 5 (**Figure 2A**). We then plated the embryoid bodies onto matrigel-coated dishes and grew them in a medium supplemented with N2. After 5–7 days in culture, attached EBs differentiated into rosettes (**Figure 2B**) which expressed the early neural precursor marker Nestin (**Figure 2C**). Rosettes were then dissociated with Accutase or manually picked, plated in matrigel-coated dishes and maintained as neural progenitors using a medium containing N2, B27, bFGF, and EGF. We purified a homogeneous population of hNPs using anti-PSA-NCAM microbeads and magnetic-based separation (Kim et al., 2012) (**Figure 2D**).

All purified hNPs were positive for the neural cell markers Nestin, Pax6 and Sox2 (**Figures 2E–H**) and the majority of the cells were positive for Ki67, strongly demonstrating that they are self-renewing (**Figure 2F**); βTubIII positive cells were present, in accordance with previous reports (Elkabetz and Studer, 2008; Kim et al., 2012) (**Figure 2I**), and we didn't detect positivity for the neuron-specific protein MAP2 (**Figures 2J,K**) and the myoepithelial marker αSMA (**Figure 2L**). In addition, hNPs did not express the pluripotency markers Nanog OCT3/4 and Tra-1-81 (**Figures 2M,N**).

hNPs were kept under proliferating conditions in the presence of bFGF and EGF and were stable in morphology and for the expression of Nestin for more than 30 passages (data not shown). Moreover, hNPs could be successfully infected with lentiviruses expressing different proteins. We thus obtained different hNP clones expressing EGFP under CMV and Synapsin promoters (see **Figure 4**, SYN-GFP), RFP under CMV promoter, PSD-95-GFP (not shown) and GFP-Homer1b under CMV promoters (see **Figure 8**, HOMER-GFP). All clones were extensively expanded, frozen and thawed without losing their ability to further differentiate into neurons up to passage 16. The large majority of the cells were positively stained for Nestin and only a very small number of them were also positive for the astroglial marker GFAP (**Figure A2**).

TERMINAL NEURONAL DIFFERENTIATION OF hNPs

To differentiate hNPs into functional neurons, we compared three different protocols: we cultured the hNPs on E18 rat primary cortical neurons (first method), on rat primary glial cells (second

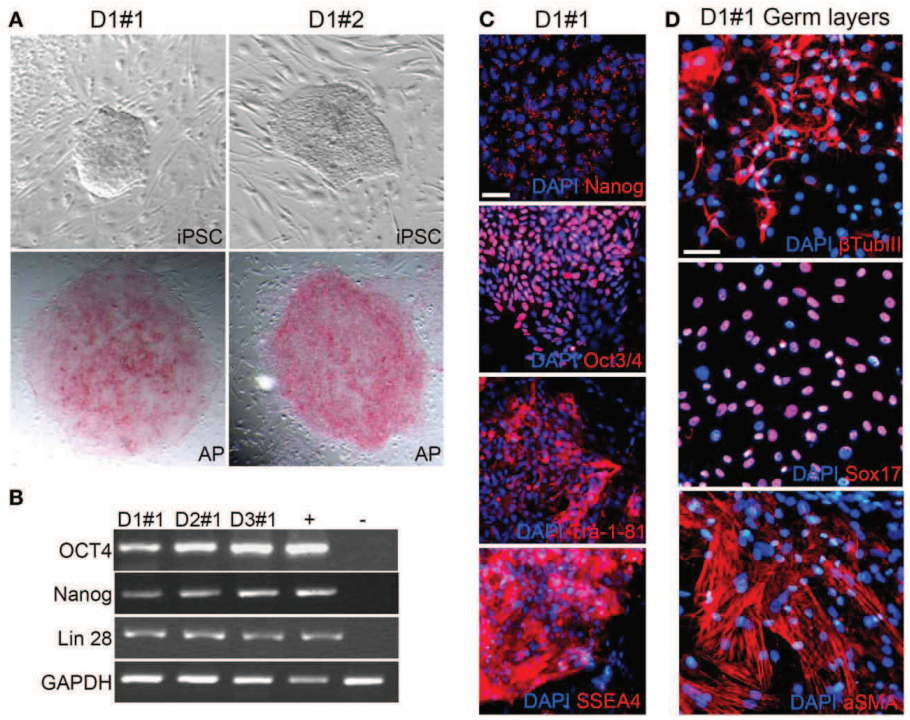

FIGURE 1 | Generation of hiPSC colonies. (A) Representative images of established hiPSC colonies, clones are positive for phosphatase alkaline. **(B)** and **(C)** iPSC clones show expression of pluripotency markers. **(D)** iPSCs differentiate into the three germ layers *in vitro,* ectoderm (+βTubulin III), endoderm (+Sox17) and mesoderm (+aSMA). Scale bar, 50 μm.

method) or simply on matrigel (third method). In order to characterize the best and fastest method to induce hNP differentiation, each condition was analyzed and compared for morphology and electrophysiological properties at 20, 50, and 60 days after plating.

For the culture on E18 rat primary cortical neurons, hNPs were first infected with a lentivirus expressing EGFP under either the CMV (EGFP-hNPs) or Synapsin promoter, then plated onto cortical neurons at DIV7 (10,000–60,000 infected hNPs were plated in one well of a twelve well plate containing 75,000 primary neurons). Neuronal medium (Romorini et al., 2004) was changed every 4 days until the end of differentiation.

The hNP-derived cells could be distinguished from rat neurons based on GFP expression or by labeling them with human-specific antibodies. When infected with EGFP under the Synapsin promoter, neurons expressed GFP after 30 days in culture.

After 20–60 days of differentiation, we evaluated the hNP-derived mature neuronal cells using specific markers visualized by immunofluorescence. The hNP-derived neurons, displaying green fluorescence, all expressed nuclear NeuN (**Figure 3A**), a classical marker of neuronal cell types; interestingly, immunoreactivity for NeuN is only observed in neurons that have become postmitotic, whereas no staining is observed in proliferative zones (Mullen et al., 1992). All green cells also expressed the human nuclei protein (hNa), demonstrating that the neuronal cells we obtained derived from human cells (**Figure 3A**). As the infection efficiency of the EGFP-expressing lentivirus was lower than 100%, some non-green cells were also positive for hNa. We analyzed neuronal differentiation by immunofluorescence using MAP2 for labeling dendrites and VGLUT and Synaptophysin (Syn) for labeling synapses. hNP-derived neurons had elaborate dendritic arbors and many Synaptophysin-positive puncta, and VGLUT positive puncta were detected starting around day 60 of differentiation (**Figure 3A** bottom). We observed that the majority of the neurons generated from hNP cell cultures were MAP2 and VGLUT positive neurons, and we basically did not detect MAP2 and GABA double-positive cells (data not shown), indicating that we mainly obtained excitatory neurons.

We recorded total ionic currents, discharges induced by injection of depolarizing currents, and spontaneous postsynaptic currents. Recordings of total ionic currents showed that hNPs cultured on E18 rat primary cortical neurons were able, after 60 days in culture, to generate cells displaying voltage-gated potassium currents and, most importantly, voltage-gated sodium currents blocked by the application of the selective blocker tetrodotoxin (TTX), which is a specific feature of mature neurons (**Figure 3B**). These cells were excitable and displayed discharges of action potentials lasting for the entire duration of the 400 ms step of injected depolarizing current (**Figure 3C**). In order to determine whether hNP-derived neurons expressed functional neurotransmitter receptors and formed functional synapses, we recorded spontaneous glutamatergic and GABAergic postsynaptic currents (excitatory postsynaptic currents, EPSCs and inhibitory postsynaptic currents, IPSCs). EPSC were recorded

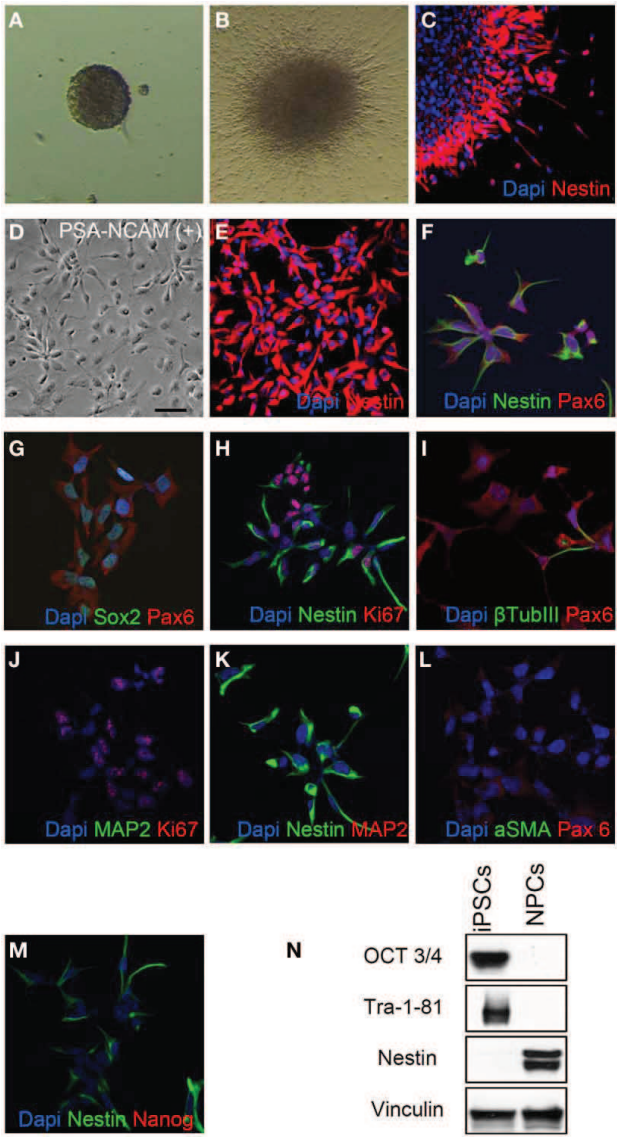

FIGURE 2 | Generation of neural progenitor cells (hNPs). (A,B) Representative images of embryoid bodies **(A)** and rosettes **(B)**. **(C)** Rosettes are positive for the early neural precursor marker Nestin. **(D)** This representative image shows the typical morphology of PSA-NCAM positive purified hNPs, **(E–H)** Most of PSA-NCAM positive cells are positive for Nestin, Pax6 and Sox2, typical hNP makers; they are also positive for Ki67 confirming that they are self-renewing. **(I)** about 5% of cells are positive for βTubulin III. **(J–L)** hNPs do not express MAP2 and αSMA, markers of mature neurons and mesodermal cells respectively. **(M,N)** hNPs do not express the pluripotency markers Nanog, OCT3/4 and Tra-1-81. Scale bar, 50 μm.

at a potential of −70 mV, IPSCs at a potential of +30 mV. We were able to record EPSCs that were blocked by application of kynurenic acid (**Figure 3D**); on the contrary, we have never observed GABAergic postsynaptic currents in these conditions (**Figure 3E**).

We next investigated whether we could differentiate hNPs using rat primary glial cells as feeders. hNPs were first infected with a lentivirus expressing EGFP under the Synapsin promoter, then 10,000–40,000 infected hNPs were plated in one well of a twelve well plate containing 75,000 glial cells. When infected with EGFP under the Synapsin promoter, neurons expressed GFP after 30 days in culture. After 60 days differentiated cells, green, were positive for hNa, but also for neuronal and synaptic markers such as MAP2, synaptophysin and VGLUT (**Figure 4A**).

Again we recorded total ionic currents, discharges induced by injection of depolarizing current, and spontaneous postsynaptic currents. hNPs, cultured on primary glial cells, were able to generate neuronal cells displaying voltage-gated potassium currents and, most importantly, voltage-gated sodium currents blocked by the application of TTX (**Figures 4B,C**).

Using the voltage-clamp configuration we also recorded spontaneous glutamatergic postsynaptic currents (**Figure 4D**), but we never observed GABAergic postsynaptic currents (**Figure 4E**). Finally, we differentiated hNPs into neurons in the absence of feeder cells. 4000 hNPs were plated onto matrigel-coated coverslips and grown in hNP medium without bFGF and EGF for up to 60 days. The medium was changed two times a week. As shown in **Figure 5A**, total cell extracts were analyzed by western blot at day 0, 14, and 50 of differentiation. At day 14 they were positive for βTubulin III and PSD-95, while the expression of Nestin was reduced, and synaptic development continued until day 50, as shown by the increasing levels of synaptophysin and PSD-95. hNP-derived neurons were also analyzed by immunofluorescence at day 50 and the majority of cells were positive for the neuronal markers βTubulin III and MAP2 (**Figure 5B**).

Similar to the previous differentiation methods, neurons from these cultures displayed voltage-gated sodium currents blocked by the application of TTX and voltage-gated potassium currents (**Figure 5C**) and were excitable (**Figure 5D**). We recorded spontaneous glutamatergic postsynaptic currents (EPSCs) (**Figure 5E**), but we never observed GABAergic postsynaptic currents in these conditions (**Figure 5F**) although we found some spare neurons positive for GABA (**Figure 5B**, bottom panels).

Thus, in order to improve the differentiation of GABAergic neurons, we plated EGFP-hNPs onto rat cortical neurons as previously described and treated the coculture with 1μ M retinoic acid starting 24 h after plating (Addae et al., 2012). After 60 days of differentiation, we stained the hNP-derived mature neuronal cells using an anti-GAD67 antibody to detect GABAergic neurons and observed a MAP2, GAD67, and VGAT positive population of cells (**Figures 6A,B**). In these cultures we recorded voltage-gated sodium and potassium currents (**Figure 6C**), action potential discharges (**Figure 6D**), as well as both excitatory and inhibitory postsynaptic currents (**Figures 6E,F**), showing that retinoic acid promotes the differentiation of GABAergic neurons.

The efficiency of terminal differentiation expressed as percentage of neurons and glial cells among the total number of hNPC plated was: 25% of neurons and 5% of glial cells with rat primary neurons, 6% of neurons and 5% of glial cells on matrigel in neuronal differentiating medium and 17% of neurons and 5% of glial cells on coculture with rat glial cells. These data suggest that the rate and the speed of differentiation of hNPCs were strictly dependent on the strategy used that has a greatest influence on

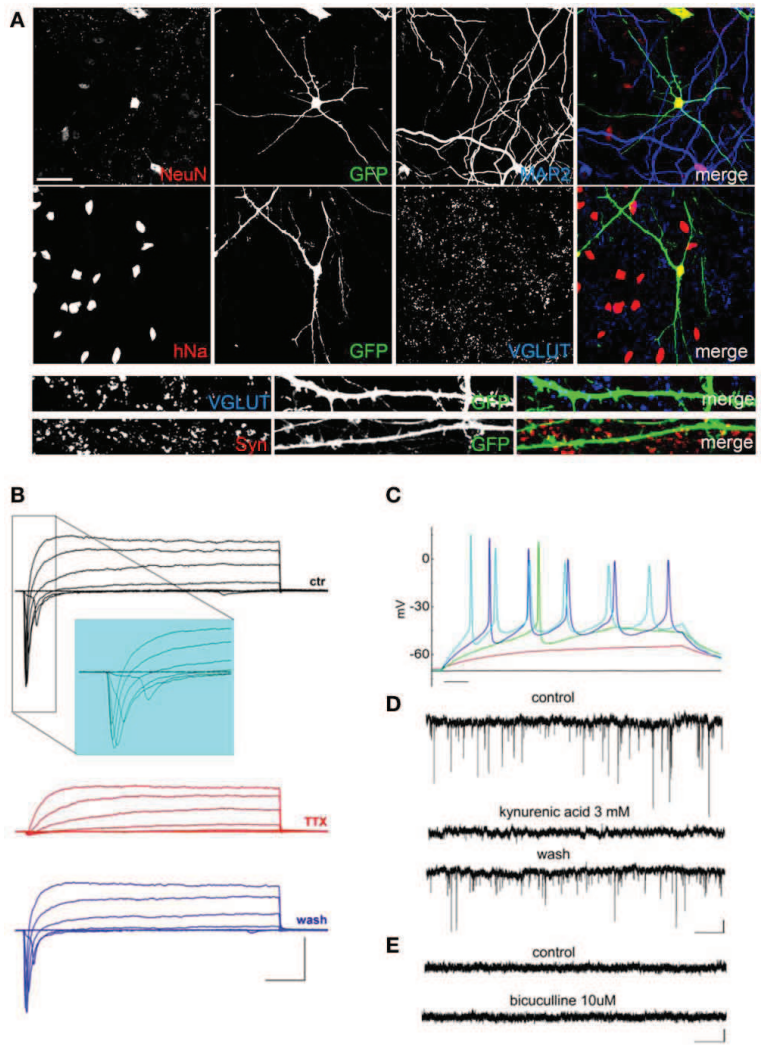

FIGURE 3 | Characterization of hNP-derived neurons differentiated by coculture on E18 rat primary cortical neurons. (A) hNP-derived neurons are positive for MAP2 and hNA and are also positive for the mature neuronal markers NeuN (red, top, scale bar 50 μm), VGLUT (blue), and synaptophysin (red, bottom, scale bar 15 μm). **(B)** Representative total ionic current traces recorded with depolarizing voltage steps between-70 and + 10 mV (10 mV increments from a holding potential of −70 mV) from hNP-derived neurons. From top to bottom: currents in control (black), with perfusion of tetrodotoxin 1 μM (red) and after washout (blue). Scale bars, 10 ms, 1000 pA. The inset shows an enlargement of the traces in control, for better displaying voltage gated sodium currents. **(C)** Representative firing traces recorded from hNP-derived neurons during application of 1 s injections of depolarizing current steps from a holding potential of −70 mV. Scale bar, 100 ms. **(D)** Traces showing spontaneous excitatory postsynaptic currents (EPSCs) recorded from hNP-derived neurons. From top to bottom: EPSCs recorded at the holding potential of −70 mV in the presence of 10 μM bicuculline, during perfusion of bicuculline and 3 mM kynurenic acid (which blocked the activity), and after washout of kynurenic acid. Scale bars, 10 pA, 1 s. **(E)** Current traces acquired at the holding potential of +30 mV with 3 mM kynurenic acid for recording spontaneous inhibitory (GABAergic) postsynaptic currents (IPSCs), which we did not observe. From top to bottom: current traces before and after application of 10 μM bicuculline. Scale bars, 10 pA, 1 s.

neuronal differention than on glial differentiation. We also found that in absence of retinoic acid we obtained only glutamatergic excitatory neurons, while in presence of the drug during the differentiation protocols about 15% of the neurons obtained were inhibitory GABAergic neurons.

MORPHOLOGICAL AND ELECTROPHYSIOLOGICAL COMPARISON BETWEEN DIFFERENTIATION PROTOCOLS

We then compared the three developmental protocols considering dendrite development, formation of dendritic spines and synapses, and electrophysiological properties. At 20, 50, and 60 days we measured the number of dendrites and their mean length. Interestingly, we found that both number of dendrites and mean length were not significantly different between different ages of development and different differentiation protocols (**Figure 7**; **Table 1**). Only the dendritic mean length of hNP-derived neurons grown on matrigel after 20 days of culture are statistically smaller compare to hNP-derived neurons grown with the other protocols (**Table 1**). We then measured the number of dendritic spines, as a measure of synapse formation, during development. Opposite

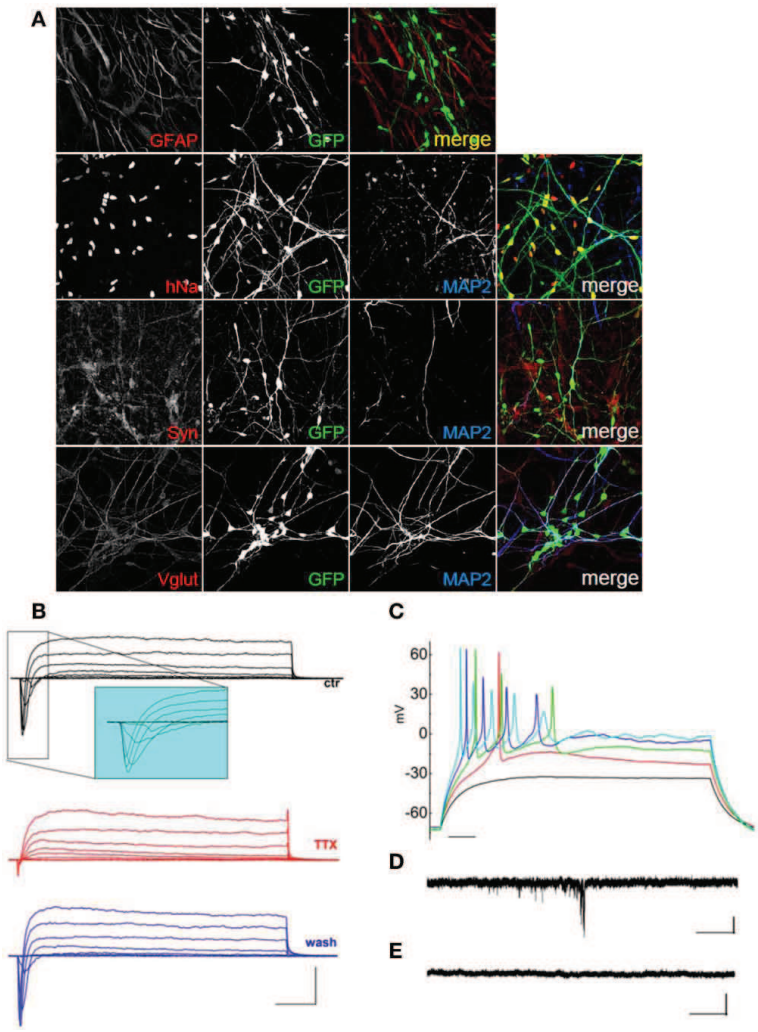

FIGURE 4 | Characterization of hNP-derived neurons differentiated by co-culture on rat glial cells. (A) hNP-derived neurons are positive for hNA (red; top, left) and MAP2 (blue) and for the mature neuronal markers synaptophysin (red, middle, left) and VGLUT (red, bottom, left). Scale bar, 50 μm. **(B)** Representative total ionic current traces recorded with depolarizing voltage steps between −70 and +10 mV (10 mV increments from a holding potential of −70 mV) from hNP-derived neurons. From top to bottom: currents in control (black), with perfusion of tetrodotoxin 1 μM (red) and after washout (blue). Scale bars, 10 ms, 500 pA. The inset shows an enlargement of the traces in control, for better displaying voltage gated sodium currents. **(C)** Representative firing traces recorded from hNP-derived neurons during application of 1 s injections of depolarizing current steps from a holding potential of −70 mV. Scale bar, 100 ms. **(D)** Traces showing spontaneous excitatory postsynaptic currents (EPSCs) recorded from hNP-derived neurons. EPSCs recorded at the holding potential of −70 mV in the presence of 10 μM bicuculline. Scale bars, 10 pA, 1 s. **(E)** Current traces acquired at the holding potential of + 30mV with 3 mM kynurenic acid for recording spontaneous inhibitory (GABAergic) postsynaptic currents (IPSCs), which we did not observe. Scale bars, 10 pA, 1 s.

to dendritic development, we were not able to measure dendritic spines and synaptic protein clusters earlier than 50 days in culture, indicating that synapse maturation occurs later in already developed dendrites. Interestingly, when we compared the three different developmental protocols, we found that at the same culture age the hNP-derived neurons grown on rat primary cortical neurons had more dendritic spines and more synapses compared to the other two protocols (at 50 days in culture we measured a mean of 1.7 ± 0.4 spines per 10 μm on hNP-derived neurons grown on rat primary cortical neurons, a mean of 0.3 ± 0.1 spines per 10 μm on hNP-derived neurons grown on matrigel and a mean 0.4 ± 0.2 spines per 10 μm on hNP-derived neurons grown on glial cells; at 60 days in culture we measured a mean of 3.6 ± 1.1 spines per 10 μm on hNP-derived neurons grown on rat primary cortical neurons, a mean of 0.6 ± 0.3 spines per 10 μm on hNP-derived neurons grown on matrigel, and a mean 1.6 ± 0.4 spines per 10 μm on hNP-derived neurons grown on glial cells).

As mentioned before, recordings of total ionic currents showed that after 50–60 days in culture all of the terminal differentiation conditions were able to generate hNP-derived cells displaying voltage-gated sodium currents, which is a specific feature of

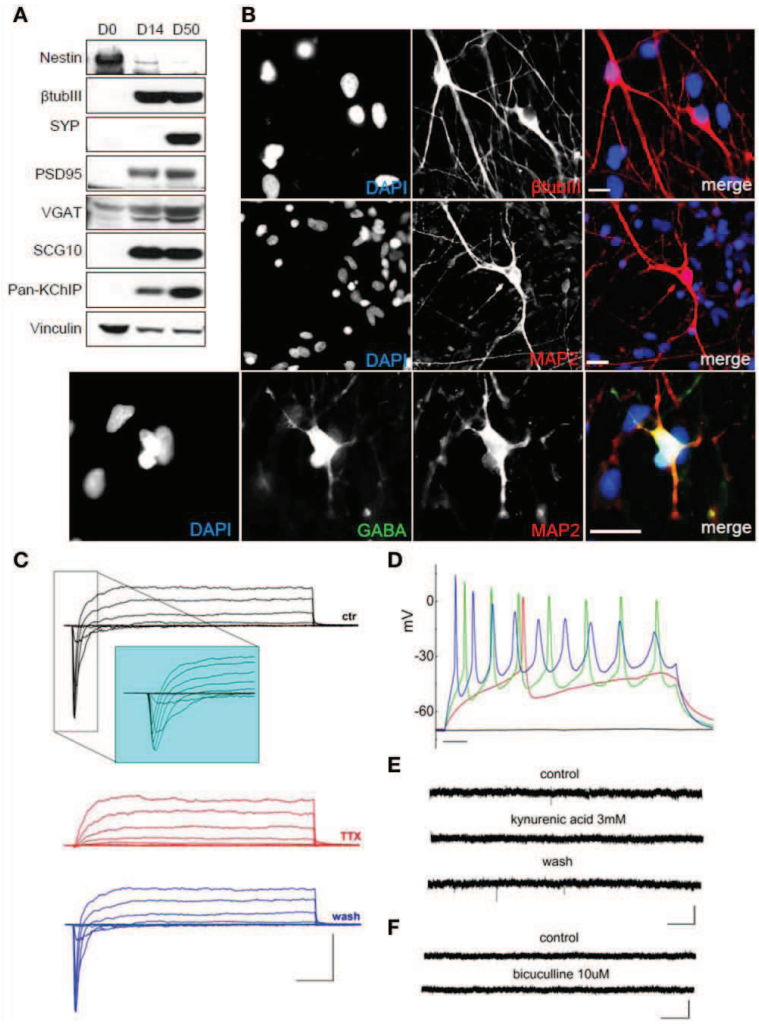

FIGURE 5 | Characterization of hNPC-derived neurons grown on matrigel in differentiation medium. (A) During differentiation of hNPs, the neural precursor marker Nestin is downregulated while the neuronal marker βTubIII is upregulated. hNP-derived neurons express the pre-synaptic marker synaptophysin, the postsynaptic marker PSD-95, the inhibitory synapse marker VGAT, the neuronal growth-associated protein SCG10 and the K^+ channel interacting proteins KChIP. **(B)** hNP-derived neurons are positive for the neuronal markers βTubIII (red, top), MAP2 (red, middle and bottom) and GABA (green). Scale bar, 20 μm. **(C)** Representative total ionic current traces recorded with depolarizing voltage steps between −70 and + 10 mV (10 mV increments from a holding potential of −70 mV) from hNP-derived neurons. From top to bottom: currents in control (black), with perfusion of tetrodotoxin 1 μM (red) and after washout (blue). Scale bars, 10 ms, 500 pA. The inset shows an enlargement of the traces in control, for better displaying voltage gated sodium currents. **(D)** Representative firing traces recorded from hNP-derived neurons during application of 1 s injections of depolarizing current steps from a holding potential of −70 mV. Scale bar, 100 ms. **(E)** Traces showing spontaneous excitatory postsynaptic currents (EPSCs) recorded from hNP-derived neurons. From top to bottom: EPSCs recorded at the holding potential of −70mV in the presence of 10 μM bicuculline, during perfusion of bicuculline and 3 mM kynurenic acid (which blocked the activity), and after washout of kynurenic acid. Scale bars, 10 pA, 1 s. **(F)** Current traces acquired at the holding potential of + 30 mV with 3 mM kynurenic acid for recording spontaneous inhibitory (GABAergic) postsynaptic currents (IPSCs), which we did not observe. From top to bottom: current traces before and after application of 10 μM bicuculline. Scale bars, 10 pA, 1 s.

mature neurons (**Figures 3B**, **4B**, **5C**, **6C**; **Table 1**). Considering only the cells that displayed sodium currents, transient peak sodium inward currents had on average similar amplitude in the different conditions: maximal peak current density was 103 ± 13 pA/pF ($n = 17$) in cocultures with primary cortical neurons, 108 ± 20 pA/pF ($n = 9$) in cocultures with primary cortical neurons incubated with retinoic acid; 81 ± 21pA/pF ($n = 8$) in cocultures with glial cells, and 93.5 ± 13.2 pA/pF ($n = 11$) with differentiation medium (no statistically significant difference: Kruskall-Wallis test). However, the fraction of hNP-derived cells recorded after 50–60 days in culture which showed appreciable sodium current was different according to the differentiation protocol: 17/17 cells when co-cultured with rat primary neurons without retinoic acid, 9/9 when co-cultured with rat primary neurons in the presence of retinoic acid, 8/10 cells when co-cultured with glial cells, and 11/26 when they were grown in matrigel in differentiation medium ($p < 0.01$; Freeman-Halton extension of Fisher's exact test).

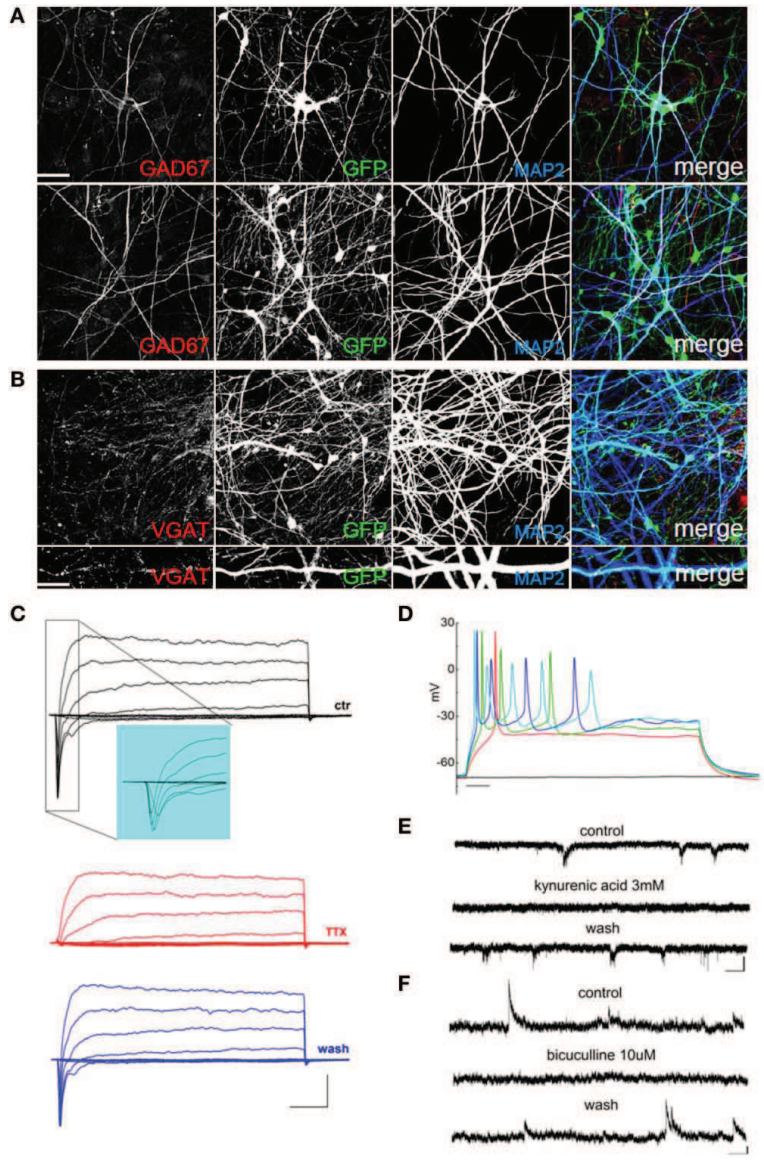

FIGURE 6 | Retinoic acid-induced differentiation of hNPs into GABAergic neurons. (A) hNP-derived neurons are positive for MAP2 and for the GABAergic marker GAD67 (red; left). Scale bar, 50 μm. **(B)** hNP-derived neurons are positive for MAP2 and the GABAergic marker VGAT. Scale bar, 15 μm. **(C)** representative total ionic current traces recorded with depolarizing voltage steps between −70 and + 10 mV (10 mV increments from a holding potential of −70 mV) from hNP-derived neurons. From top to bottom: currents in control (black), with perfusion of tetrodotoxin 1 μM (red) and after washout (blue). Scale bars, 10 ms, 500 pA. The inset shows an enlargement of the traces in control, for better displaying voltage gated sodium currents. **(D)** Representative firing traces recorded from hNP-derived neurons during application of 1 s injections of depolarizing current steps from a holding potential of −70 mV. Scale bar, 100 ms. **(E)** Traces showing spontaneous excitatory postsynaptic currents (EPSCs) recorded from hNP-derived neurons. From top to bottom: EPSCs recorded at the holding potential of−70 mV in the presence of 10 μM bicuculline, during perfusion of bicuculline and 3 mM kynurenic acid (which blocked the activity), and after washout of kynurenic acid. Scale bars, 10 pA, 1 s. **(F)** Traces showing spontaneous inhibitory (GABAergic) postsynaptic currents (IPSCs) recorded from hNP-derived neurons. From top to bottom: current traces recorded at the holding potential of +30mV in the presence of 3 mM kynurenic acid, during perfusion of kynurenic acid and 10 μM bicuculline (which blocked the activity), and after washout of bicuculline. Scale bars, 10 pA, 1 s.

hNP-derived neurons were also able to produce fire discharges of action potentials in response to injection of depolarizing current steps; in order to compare them in the same condition, we maintained their resting potential at −70 mV injecting the appropriate holding current. All the cells displaying appreciable sodium current were excitable and generated overshooting action potentials (**Figures 3C**, **4C**, **5D**, **6D**), which is a further specific feature of mature neurons.

Consistently with the morphological data, we recorded spontaneous synaptic activity at 50–60 days in hNP-derived neurons

Table 1 | Quantitative comparison between differentiation protocols.

	20 days	50 days	60 days
NUMBER OF DENDRITES, MEAN LENGHT IN μm (n. of Cells Analyzed)			
Coculture with rat primary neurons	3.2 ± 1.1 82.2 ± 8.5 (*n* = 24)	3.7 ± 1.1 86.1 ± 7.4 (*n* = 30)	3.2 ± 1.1 78.4 ± 9.3 (*n* = 21)
Coculture with rat primary neurons with RA	nm	3.3 ± 0.8 81.2 ± 8.5 (*n* = 27)	3.1 ± 1.4 84.4 ± 6.8 (*n* = 18)
Culture on matrigel in neuronal differentiating medium	3.8 ± 0.8 52.3 ± 4.5 *(*n* = 19)	4.0 ± 0.7 79.5 ± 4.6 (*n* = 19)	4.3 ± 1.5 83.8 ± 7.6 (*n* = 21)
Coculture with rat glial cells	nm	3.5 ± 0.8 90.6 ± 6.9 (*n* = 28)	2.8 ± 1.6 88.5 ± 9.8 (*n* = 26)
NUMBER OF DENDRITIC SPINES PER 10 μm (n. of Cells Analyzed)			
Coculture with rat primary neurons	0 (*n* = 14)	1.7 ± 0.4 (*n* = 10)	3.6 ± 1.1 (*n* = 11)
Coculture with rat primary neurons with RA	nm	nm	2.9 ± 0.6 (*n* = 8)
Culture on matrigel in neuronal differentiating medium	0 (*n* = 19)	0.3 ± 0.1 **(*n* = 12)	0.6 ± 0.3 **(*n* = 14)
Coculture with rat glial cells	0 (*n* = 9)	0.4 ± 0.2 **(*n* = 10)	1.6 ± 0.4 **(*n* = 10)
% OF CELLS WITH APPRECIABLE SODIUM CURRENT (n. of Cells Analyzed)			
Coculture with rat primary neurons	nm	100% (*n* = 11)	100% (*n* = 6)
Coculture with rat primary neurons with RA	nm	100% (*n* = 9)	nm
Culture on matrigel in neuronal differentiating medium	0% (*n* = 15)	21.4% **(*n* = 14)	66.6% **(*n* = 12)
Coculture with rat glial cells	nm	nm	80% **(*n* = 10)

*$p < 0.05$ compare to c. with rat primary neurons. nm, non measured.
**$p < 0.01$ compare to c. with rat primary neurons. nm, non measured.

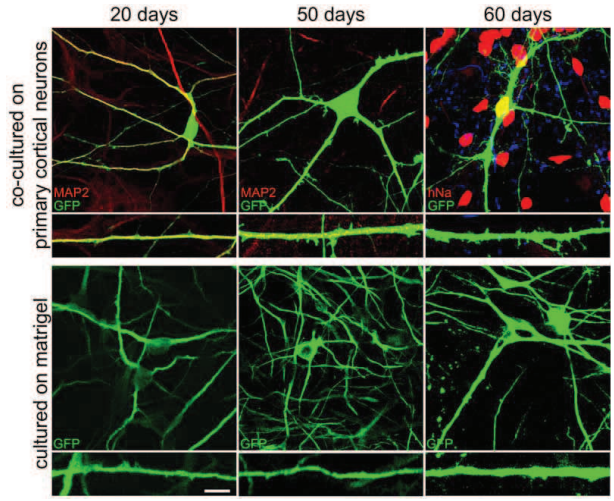

FIGURE 7 | Morphological comparison of neurons obtained with different differentiation protocols. The panels show representative images of neurons and dendrites of hNP-derived neurons which have been differentiated by co-culture on E18 rat primary cortical neurons or on matrigel after 20, 50, and 60 days in culture.

obtained with all the differentiation protocols, showing that they can form active networks. However, the frequencies of excitatory postsynaptic currents were higher in co-cultures with primary cortical rat neurons (average frequency in recordings of 125 s: 0.40 ± 0.13 Hz without retinoic acid, $n = 15$ cells; 0.23 ± 0.17 Hz without retinoic acid, $n = 5$ cells) compared to cells co-cultured with glia or grown on matrigel in differentiation medium (0.02 ± 0.01 Hz, $n = 5$ cells, 0.03 ± 0.01 Hz, $n = 5$ cells, respectively; $p < 0.05$ Kruskall-Wallis test).

To follow-up synapses formation during neuronal differentiation onto cortical neurons (the protocol that we considered the best for synapse formation), hNPs were infected with a lentivirus expressing Homer-GFP under CMV promoter. After 56 days of differentiation, the Homer-GFP signal was strong and diffused through the entire neuron indicating that, even in the presence of synapses and dendritic spines (**Figure 7**; **Table 1**), at this stage neurons are not sufficiently mature to cluster Homer at excitatory synapses. Only after 88 days in co-culture the Homer-GFP signal clustered with the classical synapses distribution (**Figures 8A,B**), suggesting that even if they are electrophysiologically active after 60 days in co-culture, these neurons need more time to develop more morphologically mature postsynapses.

DISCUSSION

Various studies have demonstrated the ability to generate neural stem cells (NSCs) from different sources such as hESCs, iPSCs or fibroblasts (Hochedlinger and Plath, 2009; Miura et al., 2009; Fong et al., 2010; Zhou et al., 2010; Kim et al., 2011; Peljto and Wichterle, 2011; Eiraku and Sasai, 2012; Han et al., 2012; Lujan et al., 2012; Sheng et al., 2012; Thier et al., 2012; Yamanaka, 2012).

Here we describe the establishment of replicating human neural-precursor cell lines, hNPs, from hiPSCs and their differentiation into mature neurons with different protocols, showing

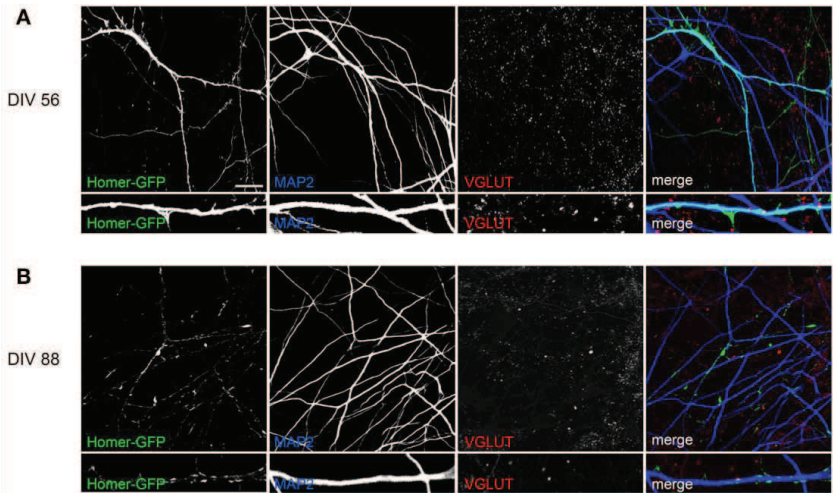

FIGURE 8 | Characterization of postsynapse formation in hNP-derived neurons differentiated by co-culture on E18 rat primary cortical neurons. (A) After 56 days in co-culture, hNP-derived neurons are positive for MAP2 but the Homer-GFP signal is spread throughout the entire neuron. Scale bar, 50 μm. **(B)** After 88 days of co-culture, hNP-derived neurons are positive for MAP2 and the Homer-GFP signal is clustered with the classical synapse distribution. Scale bar, 15 μm.

that they display different developmental properties *in vitro*, depending on the protocol used. The great difference between hiPSCs and hESCs is that, even they are both human stem cells, only hiPSCs can be collect from patients representing a unique model of pathology. For this reason we decided to analyse only neuronal differentiation of hNPC derived by hiPSC without considering hESC as control because the main aims of our project was to develop protocol suitable for hiPSCs.

Our hNP lines were obtained by inducing the neural phenotype through the generation of EBs and rosettes. hNPC were obtained by EBs formation instead of using dual SMAD inhibitors because we found that the EBs method is cheaper and more reproducible (Marchetto et al., 2010; Tang et al., 2013; Yuan et al., 2013). These hNPs did not express markers of pluripotency such as OCT 3/4 and Tra-1-81 and Nanog while expressing Nestin, an early neural lineage marker (**Figures 2C–N**) which was progressively lost following the induction of terminal differentiation (**Figure 5A**). The expression of Nestin, however, was maintained for up to 30 passages in all hNP cells, with only a minority of them being also positive for the glial marker GFAP, suggesting that the hNP lines are stable and do not spontaneously differentiate when grown in a medium containing bFGF and EGF (see Materials and Methods).

In all three *in vitro* protocols we used to differentiate hNPs we were able to obtain functional neurons that could be studied biochemically (when grown on matrigel), morphologically and electrophysiologically. Interestingly, the best neuronal maturation—measured as amount of dendritic spines, mature synapse, synaptic activity and fraction of recorded cells with appreciable sodium current—was obtained when we co-cultured the hNPs with primary rat cortical neurons. This might indicate that hNP-derived neurons can form synapses with rat neurons, or that the direct contact with rat neurons and/or the conditioned medium of the primary culture better support the differentiation of hNP cells. To note, we may exclude the latter possibility because we were not able to induce the same differentiation by simply using the primary culture conditioned medium (data not shown).

It's relevant to underline that the overall dendritic development was not differentially regulated by the different protocol used. As shown in **Table 1**, the number and mean length of dendrites was not statistically different between the different protocols used already after 20 days. Indeed our data suggest that dendritic development is already complete at 20 days, although these neurons are not electrophysiologically mature (**Table 1**). Thus, our results suggest that in these cultures neuronal dendrite formation occurs largely before the functional expression of sodium channels and the formation of synapses, and does not depend on the differentiation methods. Interestingly, during the synapse maturation period we didn't observe any further development of the dendritic arborization, suggesting that these two differentiation processes are mostly independent. Overall, our results show that the co-culture with primary cortical neurons is a condition that favors both electrophysiological maturation and synapse formation.

Although we observed synaptic activity after 50–60 days of culture, we also showed that, in order to obtain completely mature synaptic clustering of transfected GFP-Homer1b, more than 80 days of culture were required (**Figure 8B**). This data suggests that, similarly to what demonstrated for primary neuronal cultures (Bresler et al., 2004), the assembly of the postsynaptic density occurs temporally after the formation of the pre-synaptic compartment and of a functional electrophysiologically measurable synapse. Thus, our data suggests that the greatest difference between differentiation of hNPs and primary neurons *in vitro* is the time required for maturation: weeks for hNPs, days for primary neurons. Although the long period of time required for hNP neuronal differentiation is probably an intrinsic property, our data suggest that it's possible to accelerate this process by

changing the culture environment, as in co-cultures with primary neurons.

Our data clearly suggest that the co-culture method is the most efficient to obtain mature neurons. In order to use hiPSCs as model for brain diseases is essential to differentiate them into functional neurons; our data clearly suggest that the co-culture method is the most efficient to obtain mature neurons both excitatory and inhibitory. It will be interesting to study if different type of primary neuron culture should be used to generate specific neurons subtype. The capability of our hNPs to differentiate in different subtypes of neurons is confirmed by the ability of retinoic acid to induce the maturation of inhibitory neurons (Addae et al., 2012). The differentiation potential of these cells into glial cells has been also determined (data not shown).

In summary, we describe a simple culture procedure to reproducibly and efficiently generate hNP cell lines from human iPSCs. These cells self-renew rapidly and can be stimulated to mature into different subtypes of neurons. We show that the rate of differentiation is strictly dependent on the strategy used to differentiate hNP cells and that the co-culture with rat cortical neurons is the most efficient way to obtain completely functional and morphologically developed neurons. The ability to obtain mature and functional neurons from self-renewing hNPs has major implications for regenerative medicine. Moreover, these lines will provide innovative experimental platforms to investigate mechanisms of neuronal differentiation and can serve as a model system for unveiling disease pathogenesis, for drug screening and toxicity tests.

ACKNOWLEDGMENTS

This work was financially supported by Comitato Telethon Fondazione Onlus, grant no. GGP09196 and GGP11095 (to Carlo Sala) and GGP10066 (to Domenico Delia), Fondazione CARIPLO project number 2012-0593, Italian Institute of Technology, Seed Grant, Ministry of Health in the frame of ERA-NET NEURON, PNR-CNR Aging Program 2012–2014 (to Carlo Sala), LabEx ICST (to Massimo Mantegazza) and CNRS-PICS (to Massimo Mantegazza and Silvana Franceschetti).

REFERENCES

Aboud, A. A., Tidball, A. M., Kumar, K. K., Neely, M. D., Ess, K. C., Erikson, K. M., et al. (2012). Genetic risk for Parkinson's disease correlates with alterations in neuronal manganese sensitivity between two human subjects. *Neurotoxicology* 33, 1443–1449. doi: 10.1016/j.neuro.2012.10.009

Addae, C., Yi, X., Gernapudi, R., Cheng, H., Musto, A., and Martinez-Ceballos, E. (2012). All-trans-retinoid acid induces the differentiation of encapsulated mouse embryonic stem cells into GABAergic neurons. *Differentiation* 83, 233–241. doi: 10.1016/j.diff.2012.03.001

Axell, M. Z., Zlateva, S., and Curtis, M. (2009). A method for rapid derivation and propagation of neural progenitors from human embryonic stem cells. *J. Neurosci. Methods* 184, 275–284. doi: 10.1016/j.jneumeth.2009.08.015

Bresler, T., Shapira, M., Boeckers, T., Dresbach, T., Futter, M., Garner, C. C., et al. (2004). Postsynaptic density assembly is fundamentally different from presynaptic active zone assembly. *J. Neurosci.* 24, 1507–1520. doi: 10.1523/JNEUROSCI.3819-03.2004

Calahorro, F., and Ruiz-Rubio, M. (2011). *Caenorhabditis elegans* as an experimental tool for the study of complex neurological diseases: Parkinson's disease, Alzheimer's disease and autism spectrum disorder. *Invert. Neurosci.* 11, 73–83. doi: 10.1007/s10158-011-0126-1

Carlessi, L., De Filippis, L., Lecis, D., Vescovi, A., and Delia, D. (2009). DNA-damage response, survival and differentiation *in vitro* of a human neural stem cell line in relation to ATM expression. *Cell Death Differ.* 16, 795–806. doi: 10.1038/cdd.2009.10

Carlessi, L., Fusar Poli, E., De Filippis, L., and Delia, D. (2013a). ATM-deficient human neural stem cells as an *in vitro* model system to study neurodegeneration. *DNA Repair* 12, 605–611. doi: 10.1016/j.dnarep.2013.04.013

Carlessi, L., Fusar Poli, E., and Delia, D. (2013b). Brain and induced pluripotent stem cell-derived neural stem cells as an *in vitro* model of neurodegeneration in ataxia-telangiectasia. *Exp. Biol. Med. (Maywood)* 238, 301–307. doi: 10.1177/1535370213480703

Cestèle, S., Scalmani, P., Rusconi, R., Terragni, B., Franceschetti, S., and Mantegazza, M. (2008). Self-limited hyperexcitability: functional effect of a familial hemiplegic migraine mutation of the Nav1.1 (SCN1A) Na+ channel. *J. Neurosci.* 28, 7273–7283. doi: 10.1523/JNEUROSCI.4453-07.2008

D'aiuto, L., Di Maio, R., Heath, B., Raimondi, G., Milosevic, J., Watson, A. M., et al. (2012). Human induced pluripotent stem cell-derived models to investigate human cytomegalovirus infection in neural cells. *PLoS ONE* 7:e49700. doi: 10.1371/journal.pone.0049700

Dimos, J. T., Rodolfa, K. T., Niakan, K. K., Weisenthal, L. M., Mitsumoto, H., Chung, W., et al. (2008). Induced pluripotent stem cells generated from patients with ALS can be differentiated into motor neurons. *Science* 321, 1218–1221. doi: 10.1126/science.1158799

Eiraku, M., and Sasai, Y. (2012). Self-formation of layered neural structures in three-dimensional culture of ES cells. *Curr. Opin. Neurobiol.* 22, 768–777. doi: 10.1016/j.conb.2012.02.005

Elkabetz, Y., and Studer, L. (2008). Human ESC-derived neural rosettes and neural stem cell progression. *Cold Spring Harb. Symp. Quant. Biol.* 73, 377–387. doi: 10.1101/sqb.2008.73.052

Esposito, G., Ana Clara, F., and Verstreken, P. (2012). Synaptic vesicle trafficking and Parkinson's disease. *Dev. Neurobiol.* 72, 134–144. doi: 10.1002/dneu.20916

Farra, N., Zhang, W. B., Pasceri, P., Eubanks, J. H., Salter, M. W., and Ellis, J. (2012). Rett syndrome induced pluripotent stem cell-derived neurons reveal novel neurophysiological alterations. *Mol. Psychiatry* 17, 1261–1271. doi: 10.1038/mp.2011.180

Fong, C. Y., Gauthaman, K., and Bongso, A. (2010). Teratomas from pluripotent stem cells: a clinical hurdle. *J. Cell. Biochem.* 111, 769–781. doi: 10.1002/jcb.22775

Goslin, K., and Banker, G. (1991). *Culturing Nerve Cells*. Cambridge: MIT Press.

Han, D. W., Tapia, N., Hermann, A., Hemmer, K., Höing, S., Araúzo-Bravo, M. J., et al. (2012). Direct reprogramming of fibroblasts into neural stem cells by defined factors. *Cell Stem Cell* 10, 465–472. doi: 10.1016/j.stem.2012.02.021

Hochedlinger, K., and Plath, K. (2009). Epigenetic reprogramming and induced pluripotency. *Development* 136, 509–523. doi: 10.1242/dev.020867

Israel, M. A., Yuan, S. H., Bardy, C., Reyna, S. M., Mu, Y., Herrera, C., et al. (2012). Probing sporadic and familial Alzheimer's disease using induced pluripotent stem cells. *Nature* 482, 216–220.

Kim, D. S., Lee, D. R., Kim, H. S., Yoo, J. E., Jung, S. J., Lim, B. Y., et al. (2012). Highly pure and expandable PSA-NCAM-positive neural precursors from human ESC and iPSC-derived neural rosettes. *PLoS ONE* 7:e39715. doi: 10.1371/journal.pone.0039715

Kim, J., Efe, J. A., Zhu, S., Talantova, M., Yuan, X., Wang, S., et al. (2011). Direct reprogramming of mouse fibroblasts to neural progenitors. *Proc Natl Acad Sci U S AProc. Natl. Acad. Sci. U.S.A.* 108, 7838–7843. doi: 10.1073/pnas.1103113108

Lois, C., Hong, E. J., Pease, S., Brown, E. J., and Baltimore, D. (2002). Germline transmission and tissue-specific expression of transgenes delivered by lentiviral vectors. *Science* 295, 868–872. doi: 10.1126/science.1067081

Lujan, E., Chanda, S., Ahlenius, H., Südhof, T. C., and Wernig, M. (2012). Direct conversion of mouse fibroblasts to self-renewing, tripotent neural precursor cells. *Proc. Natl. Acad. Sci. U.S.A.* 109, 2527–2532. doi: 10.1073/pnas.1121003109

Marcello, E., Epis, R., Saraceno, C., and Di Luca, M. (2012). Synaptic dysfunction in Alzheimer's disease.

Adv. Exp. Med. Biol. 970, 573–601. doi: 10.1007/978-3-7091-0932-8_25

Marchetto, M. C., Carromeu, C., Acab, A., Yu, D., Yeo, G. W., Mu, Y., et al. (2010). A model for neural development and treatment of Rett syndrome using human induced pluripotent stem cells. *Cell* 143, 527–539. doi: 10.1016/j.cell.2010.10.016

Miura, K., Okada, Y., Aoi, T., Okada, A., Takahashi, K., Okita, K., et al. (2009). Variation in the safety of induced pluripotent stem cell lines. *Nat. Biotechnol.* 27, 743–745. doi: 10.1038/nbt.1554

Mullen, R. J., Buck, C. R., and Smith, A. M. (1992). NeuN, a neuronal specific nuclear protein in vertebrates. *Development* 116, 201–211.

Naldini, L., Blomer, U., Gallay, P., Ory, D., Mulligan, R., Gage, F. H., et al. (1996). *In vivo* gene delivery and stable transduction of nondividing cells by a lentiviral vector. *Science* 272, 263–267. doi: 10.1126/science.272.5259.263

Paulsen, B. A. S., De Moraes Maciel, R., Galina, A., Souza Da Silveira, M., Dos Santos Souza, C., Drummond, H., et al. (2012). Altered oxygen metabolism associated to neurogenesis of induced pluripotent stem cells derived from a schizophrenic patient. *Cell Transplant.* 21, 1547–1559. doi: 10.3727/096368911X600957

Pasca, S. P., Portmann, T., Voineagu, I., Yazawa, M., Shcheglovitov, A., Pasca, A. M., et al. (2011). Using iPSC-derived neurons to uncover cellular phenotypes associated with Timothy syndrome. *Nat. Med.* 17, 1657–1662. doi: 10.1038/nm.2576

Peljto, M., and Wichterle, H. (2011). Programming embryonic stem cells to neuronal subtypes. *Curr. Opin. Neurobiol.* 21, 43–51. doi: 10.1016/j.conb.2010.09.012

Peng, H., and Chen, G. (2005). Neural precursors derived from human embryonic stem cells. *Sci. China C Life Sci.* 48, 295–299. doi: 10.1360/062004-83

Penzes, P., Cahill, M. E., Jones, K. A., Vanleeuwen, J. E., and Woolfrey, K. M. (2011). Dendritic spine pathology in neuropsychiatric disorders. *Nat. Neurosci.* 14, 285–293. doi: 10.1038/nn.2741

Reubinoff, B. E., Itsykson, P., Turetsky, T., Pera, M. F., Reinhartz, E., Itzik, A., et al. (2001). Neural progenitors from human embryonic stem cells. *Nat. Biotechnol.* 19, 1134–1140. doi: 10.1038/nbt1201-1134

Ricciardi, S., Ungaro, F., Hambrock, M., Rademacher, N., Stefanelli, G., Brambilla, D., et al. (2012). CDKL5 ensures excitatory synapse stability by reinforcing NGL-1-PSD95 interaction in the postsynaptic compartment and is impaired in patient iPSC-derived neurons. *Nat. Cell Biol.* 14, 911–923. doi: 10.1038/ncb2566

Romorini, S., Piccoli, G., Jiang, M., Grossano, P., Tonna, N., Passafaro, M., et al. (2004). A functional role of postsynaptic density-95-guanylate kinase-associated protein complex in regulating shank assembly and stability to Synapses. *J. Neurosci.* 24, 9391–9404. doi: 10.1523/JNEUROSCI.3314-04.2004

Salewski, R. P., Buttigieg, J., Mitchell, R. A., Van Der Kooy, D., Nagy, A., and Fehlings, M. G. (2013). The generation of definitive neural stem cells from PiggyBac transposon-induced pluripotent stem cells can be enhanced by induction of the NOTCH signaling pathway. *Stem Cells Dev.* 22, 383–396. doi: 10.1089/scd.2012.0218

Sheng, C., Zheng, Q., Wu, J., Xu, Z., Wang, L., Li, W., et al. (2012). Direct reprogramming of Sertoli cells into multipotent neural stem cells by defined factors. *Cell Res.* 22, 208–218. doi: 10.1038/cr.2011.175

Shi, Y., Kirwan, P., Smith, J., Robinson, H.P., and Livesey, F.J. (2012). Human cerebral cortex development from pluripotent stem cells to functional excitatory synapses. *Nat. Neurosci.* 15, 477–486, doi: 10.1038/nn.3041

Takahashi, K., and Yamanaka, S. (2006). Induction of pluripotent stem cells from mouse embryonic and adult fibroblast cultures by defined factors. *Cell* 126, 663–676. doi: 10.1016/j.cell.2006.07.024

Tang, X., Zhou, L., Wagner, A. M., Marchetto, M. C., Muotri, A. R., Gage, F. H., et al. (2013). Astroglial cells regulate the developmental timeline of human neurons differentiated from induced pluripotent stem cells. *Stem Cell Res* 11, 743–757. doi: 10.1016/j.scr.2013.05.002

Thier, M., Wörsdörfer, P., Lakes, Y. B., Gorris, R., Herms, S., Opitz, T., et al. (2012). Direct conversion of fibroblasts into stably expandable neural stem cells. *Cell Stem Cell* 10, 473–479. doi: 10.1016/j.stem.2012.03.003

Verpelli, C., Piccoli, G., Zanchi, A., Gardoni, F., Huang, K., Brambilla, D., et al. (2010). Synaptic activity controls dendritic spine morphology by modulating eEF2-dependent BDNF synthesis. *J. Neurosci.* 30, 5830–5842. doi: 10.1523/JNEUROSCI.0119-10.2010

Verpelli, C., and Sala, C. (2012). Molecular and synaptic defects in intellectual disability syndromes. *Curr. Opin. Neurobiol.* 22, 530–536. doi: 10.1016/j.conb.2011.09.007

Wernig, M., Zhao, J. P., Pruszak, J., Hedlund, E., Fu, D., Soldner, F., et al. (2008). Neurons derived from reprogrammed fibroblasts functionally integrate into the fetal brain and improve symptoms of rats with Parkinson's disease. *Proc. Natl. Acad. Sci. U.S.A.* 105, 5856–5861. doi: 10.1073/pnas.0801677105

Xia, G., Santostefano, K., Hamazaki, T., Liu, J., Subramony, S. H., Terada, N., et al. (2012). Generation of human-induced Pluripotent stem cells to model Spinocerebellar Ataxia Type 2 *in vitro*. *J. Mol. Neurosci.* 51, 237–248. doi: 10.1007/s12031-012-9930-2

Xu, L., Tan, Y. Y., Ding, J. Q., and Chen, S. D. (2010). The iPS technique provides hope for Parkinson's disease treatment. *Stem Cell Rev.* 6, 398–404. doi: 10.1007/s12015-010-9145-2

Yamanaka, S. (2012). Induced pluripotent stem cells: past, present, and future. *Cell Stem Cell* 10, 678–684. doi: 10.1016/j.stem.2012.05.005

Yin, D., Tavakoli, T., Gao, W. Q., and Ma, W. (2012). Comparison of neural differentiation potential of human pluripotent stem cell lines using a quantitative neural differentiation protocol. *Methods Mol. Biol.* 873, 247–259. doi: 10.1007/978-1-61779-794-1_16

Yuan, T., Liao, W., Feng, N. H., Lou, Y. L., Niu, X., Zhang, A. J., et al. (2013). Human induced pluripotent stem cell-derived neural stem cells survive, migrate, differentiate, and improve neurological function in a rat model of middle cerebral artery occlusion. *Stem Cell Res. Ther.* 4, 73. doi: 10.1186/scrt224

Zhang, N., An, M. C., Montoro, D., and Ellerby, L. M. (2010). Characterization of human Huntington's disease cell model from induced Pluripotent stem cells. *PLoS Curr.* 2:RRN1193. doi: 10.1371/currents.RRN1193

Zhang, S. C., Wernig, M., Duncan, I. D., Brustle, O., and Thomson, J. A. (2001). *In vitro* differentiation of transplantable neural precursors from human embryonic stem cells. *Nat. Biotechnol.* 19, 1129–1133. doi: 10.1038/nbt1201-1129

Zhou, J., Su, P., Li, D., Tsang, S., Duan, E., and Wang, F. (2010). High-efficiency induction of neural conversion in human ESCs and human induced pluripotent stem cells with a single chemical inhibitor of transforming growth factor beta superfamily receptors. *Stem Cells* 28, 1741–1750. doi: 10.1002/stem.504

Conflict of Interest Statement: The authors declare that the research was conducted in the absence of any commercial or financial relationships that could be construed as a potential conflict of interest.

Received: 30 July 2013; accepted: 18 September 2013; published online: 07 October 2013.

Citation: Verpelli C, Carlessi L, Bechi G, Fusar Poli E, Orellana D, Heise C, Franceschetti S, Mantegazza R, Mantegazza M, Delia D and Sala C (2013) Comparative neuronal differentiation of self-renewing neural progenitor cell lines obtained from human induced pluripotent stem cells. Front. Cell. Neurosci. 7:175. doi: 10.3389/fncel.2013.00175

This article was submitted to the journal Frontiers in Cellular Neuroscience.

APPENDIX

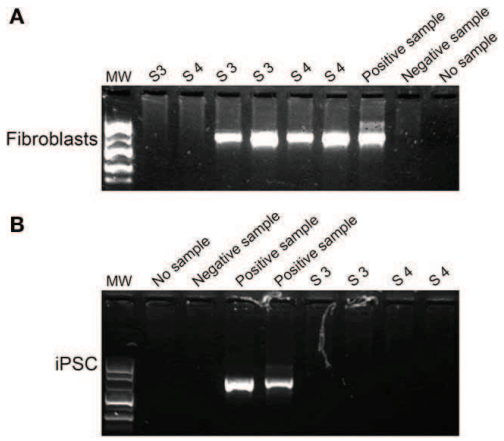

FIGURE A1 | Treatment of mycoplasma-infected fibroblasts with BM-Cyclin. The fibroblast culture medium from fibroblasts**(A)** and iPSCs **(B)** was analyzed for the presence of mycoplasma DNA using PCR before **(A)** and after **(B)** treatment for 20 days with BM-Cyclin.

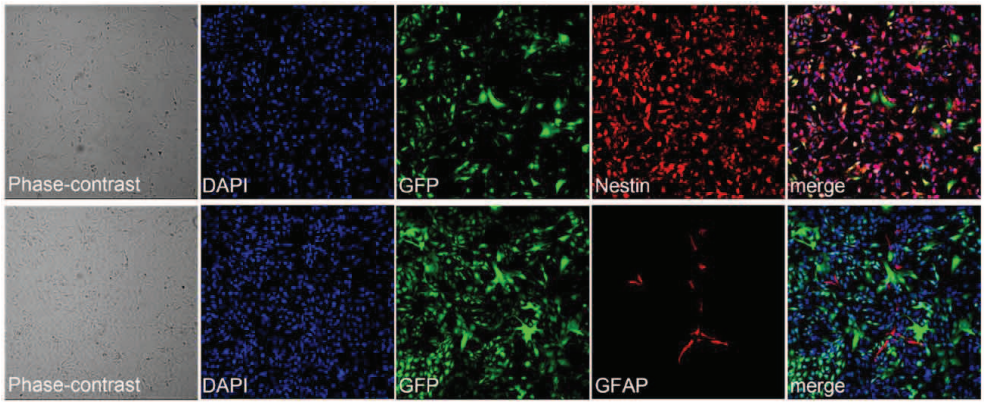

FIGURE A2 | Stem cell features of hNPs after multiple passages. After 16 passages, hNPs are still positive for Nestin (top panel). A low number of cells are positive for GFAP (bottom panel). The cells do not spontaneously differentiate during the multiple passages and maintain their stem cell nature.

OPEN

Citation: Cell Death and Disease (2013) 4, e906; doi:10.1038/cddis.2013.430

www.nature.com/cddis

Murine neural stem cells model Hunter disease *in vitro*: glial cell-mediated neurodegeneration as a possible mechanism involved

E Fusar Poli[1,2,7], C Zalfa[1,7], F D'Avanzo[3], R Tomanin[3], L Carlessi[2], M Bossi[4], L Rota Nodari[1], E Binda[1], P Marmiroli[4], M Scarpa[3,5], D Delia[2], AL Vescovi[1,5,6] and L De Filippis*[,1]

Mucopolysaccharidosis type II (MPSII or Hunter Syndrome) is a lysosomal storage disorder caused by the deficit of iduronate 2-sulfatase (IDS) activity and characterized by progressive systemic and neurological impairment. As the early mechanisms leading to neuronal degeneration remain elusive, we chose to examine the properties of neural stem cells (NSCs) isolated from an animal model of the disease in order to evaluate whether their neurogenic potential could be used to recapitulate the early phases of neurogenesis in the brain of Hunter disease patients. Experiments here reported show that NSCs derived from the subventricular zone (SVZ) of early symptomatic IDS-knockout (IDS-ko) mouse retained self-renewal capacity *in vitro*, but differentiated earlier than wild-type (wt) cells, displaying an evident lysosomal aggregation in oligodendroglial and astroglial cells. Consistently, the SVZ of IDS-ko mice appeared similar to the wt SVZ, whereas the cortex and striatum presented a disorganized neuronal pattern together with a significant increase of glial apoptotic cells, suggesting that glial degeneration likely precedes neuronal demise. Interestingly, a very similar pattern was observed in the brain cortex of a Hunter patient. These observations both *in vitro*, in our model, and *in vivo* suggest that IDS deficit seems to affect the late phases of neurogenesis and/or the survival of mature cells rather than NSC self-renewal. In particular, platelet-derived growth factor receptor-α-positive (PDGFR-α+) glial progenitors appeared reduced in both the IDS-ko NSCs and in the IDS-ko mouse and human Hunter brains, compared with the respective healthy controls. Treatment of mutant NSCs with IDS or PDGF throughout differentiation was able to increase the number of PDGFR-α+ cells and to reduce that of apoptotic cells to levels comparable to wt. This evidence supports IDS-ko NSCs as a reliable *in vitro* model of the disease, and suggests the rescue of PDGFR-α+ glial cells as a therapeutic strategy to prevent neuronal degeneration.

Cell Death and Disease (2013) **4,** e906; doi:10.1038/cddis.2013.430; published online 7 November 2013
Subject Category: Neuroscience

Mucopolysaccharidosis type II (MPSII or Hunter Syndrome) is a monogenic, X-linked inherited lysosomal storage disorder (LSD) caused by a deficit of the iduronate 2-sulfatase (IDS) enzyme, involved in glycosaminoglycan (GAG) catabolism.[1] The consequent accumulation of GAGs in all cell types induces organ impairment, with incremental neurodegeneration affecting 50–70% of patients. Death generally occurs within 20 years of age.[2] The current therapeutic strategy, enzyme replacement therapy (ERT),[3–5] is effective in peripheral organs but cannot treat brain deterioration because the recombinant enzyme does not cross the blood–brain barrier. Results in central nervous system treatment have been obtained in MPSII and MPSVII mouse models through different strategies,[6–9] but the translation to humans is hampered by risk of toxicity and immune responses.[10–13] Moreover, late diagnosis, lack of specimens from early symptomatic patients and the absence of *in vitro* models limit the elucidation of the neuro-pathogenetic events involved in the development of Hunter disease. Self-renewing neural stem cells (NSCs), capable of differentiation into neural

[1]Department of Biotechnology and Biosciences, University Milan Bicocca, Piazza della Scienza 2, Milano 20126, Italy; [2]Department of Experimental Oncology, Fondazione IRCCS Istituto Nazionale dei Tumori, Via Amadeo 42, Milano 20133, Italy; [3]Laboratory of Diagnosis and Therapy of Lysosomal Disorders, Department of Women's and Children's Health, University of Padova, Via Giustiniani 3, Padova 35128, Italy; [4]Department of Surgery and Translational Medicine, University Milano Bicocca, Via Cadore 48, Monza 20900, Italy; [5]Casa Sollievo della Sofferenza, Viale Cappuccini 2, San Giovanni Rotondo (FG) 71013, Italy and [6]Stem Cells Laboratory, Cell Factory and Biobank, Azienda ospedaliera "Santa Maria", Terni, Viale Tristano da Joannuccio 1, Terni 05100, Italy
*Corresponding author: L De Filippis, Department of Biotechnologies and Bioscience, University Milan Bicocca, Piazza della Scienza 2, Milano 20126, Italy; Tel: +39-0264483368; Fax: +39-0264483314; E-mail: lidia.defilippis@unimib.it.
[7]These authors contributed equally to this work.
Keywords: neural stem cells; MPSII; Hunter Syndrome; glial cells; lysosomal storage disorders
Abbreviations: β-tubIII, β-tubulin III; DAPI, 4′,6-diamidino-2-phenylindole dihydrochloride; Dcx, double cortin; div, days *in vitro*; ECM, extracellular matrix; EGF, epidermal growth factor; ERT, enzyme replacement therapy; FGF2, fibroblast growth factor type 2; GAG, glycosaminoglycan; GalC, galactocerebroside C; GFAP, glial fibrillary acidic protein; HD, high cell density; IDS, iduronate 2-sulfatase; IDS-ko, IDS-knockout; iPSCs, induced pluripotent stem cells; Lamp1, lysosomal-associated membrane protein 1; LD, low cell density; LSD, lysosomal storage disorder; MAP2, microtubular associated protein type2; MBP, myelin basic protein; MPSVII, mucopolysaccharidosis type VII; NSC, neural stem cell; OBs, olfactory bulbs; PDGF, platelet-derived growth factor; PDGFR, platelet-derived growth factor receptor; SVZ, subventricular zone; wt, wild type
Received 25.6.13; revised 06.9.13; accepted 23.9.13; Edited by A Verkhratsky

phenotypes, create a model for dissecting neurogenesis *in vivo* and for investigating the onset and progression of neurodegenerative diseases *in vitro*.

As the genetic defect in MPSII could compromise the neurogenic properties of NSCs,[14,15] we used NSCs derived from IDS-knockout (IDS-ko) mice to recapitulate MPSII pathogenesis. We also analyzed the relationship between IDS deficit and abnormal neurogenesis *in vivo* to clarify the mechanisms underlying the neuropathology. Our results provide a previously undocumented characterization of the IDS-ko mouse brain mirroring the pattern of a human Hunter brain, indicate glial cell-mediated neurodegeneration as a candidate mechanism involved in MPSII and validate IDS-ko NSCs as a tool to model MPSII neurodegeneration and to investigate novel therapeutic approaches.

Results

IDS deficit does not critically affect NSC self-renewal. We first established two NSC lines from the SVZ of early symptomatic C57BL6 IDS-ko mice and two NSC control lines from wild-type (wt) syngenic littermates. The identity of IDS-ko NSCs was confirmed by PCR (Supplementary Figure 1) and by IDS activity assay (Figure 1a). NSCs were expanded using the neurosphere assay[16,17] and no morphological differences were detectable between wt and IDS-ko neurospheres (Figure 1b). In the presence of both epidermal growth factor (EGF) and fibroblast growth factor type 2 (FGF2), IDS-ko and control NSCs displayed a comparable self-renewal capacity (Figure 1c), and no significant differences were evident between the viability of IDS-ko and control cells at 24, 48 and 72 h from dissociation of the

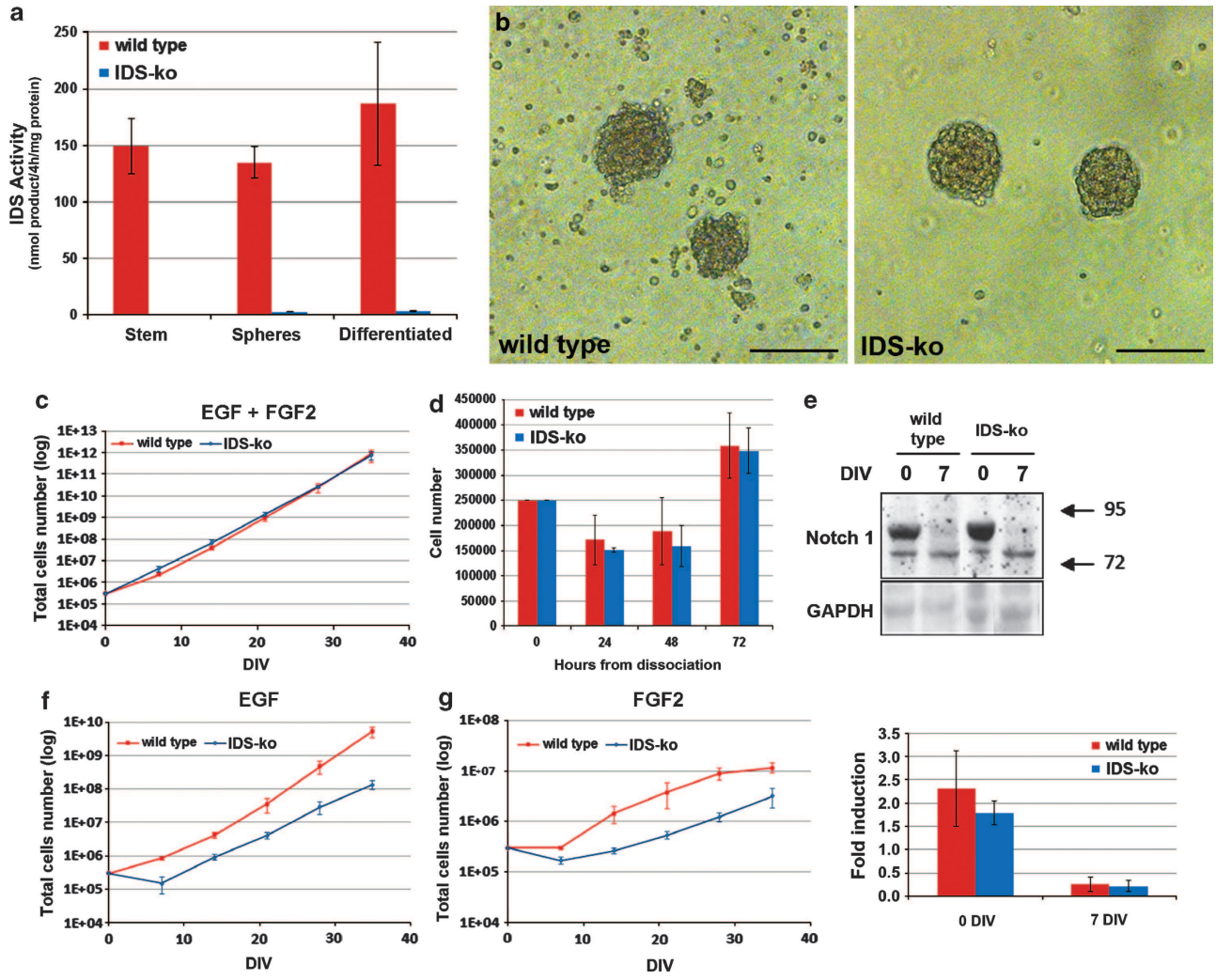

Figure 1 IDS deficit does not critically affect NSC self-renewal. **(a)** Histogram showing the IDS enzymatic activity in wt and IDS-ko NSCs. Although detectable in wt single stem cells, neurospheres and differentiated, no enzymatic activity could be revealed in IDS-ko cells. (**b**) Phase-contrast image of a free floating neurospheres culture. Scale bar: 100 μm. (**c**) Graph showing the proliferation rate of wt NSCs (red, $n=2$) and IDS-ko NSCs (blue, $n=2$) when cultured in the presence of both EGF and FGF2. (**d**) Histogram showing the number of viable wt and IDS-ko NSCs at 0, 24, 48 and 72 h after dissociation. For each line, 2.5×10^5 cells were plated ($n=2$). (**e**) Western blot analysis of Notch expression in wt and IDS-ko cells at 0 and 7 div after differentiation. (**f** and **g**) Graphs showing the proliferation rate of wt NSCs (red, $n=2$ cell lines) and IDS-ko NSCs (blue, $n=2$ cell lines) when cultured only in the presence of EGF (**f**) or in the presence of FGF2 (**g**). All results are presented as the average of the two IDS-ko and of the two wt NSC lines, respectively. Values are means ± S.E.M

neurospheres (Figure 1d). Consistently, the amount of Notch1 protein, crucial for NSC self-renewal, was comparable in wt and in IDS-ko NSCs (Figure 1e). Interestingly, in the absence of either EGF or FGF2, all NSC lines underwent a physiological progressive delay of proliferation, which appeared to be initially enhanced in IDS-ko cells (Figures 1f and g). These results suggest that IDS expression is not crucial to NSC self-renewal when EGF and FGF2 cooperate to NSC proliferation, but can affect NSC sensitivity to single mitogens possibly by altering the balance between transient amplifying progenitors and stem cells, indicating that IDS may have a role in normal differentiation of NSCs.

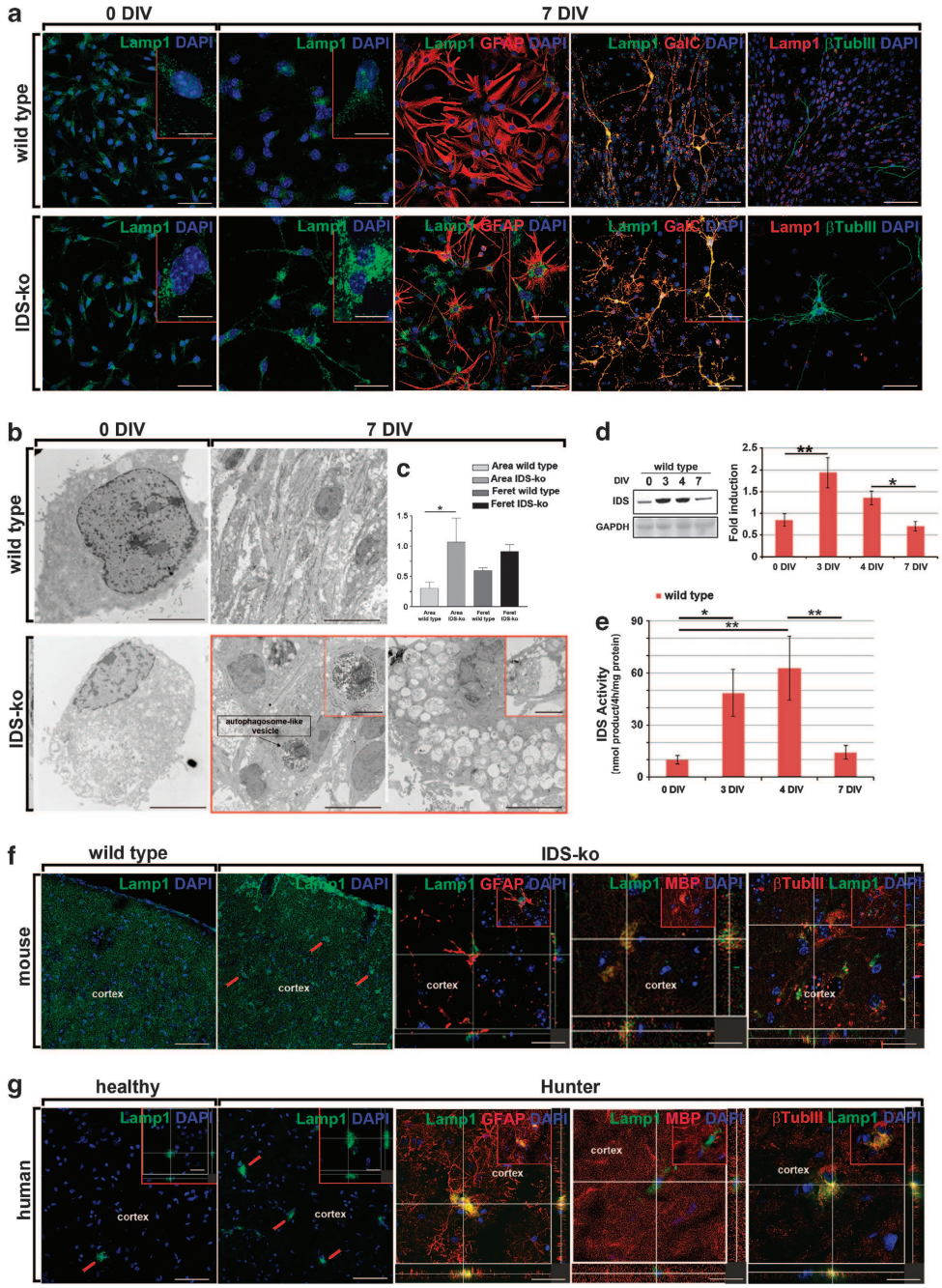

Figure 2 Lysosomal accumulation in differentiated IDS-ko NSCs and in mature neurogenic areas of both murine and human brains affected by MPSII. (**a**) Confocal microscopy images of wt and IDS-ko NSCs at 0 div and after 7 div differentiation stained against lysosome marker Lamp1 (scale bar: 10–15 m; inset scale bar: 5–8 μm). Scale bars: 75 μm: in insets: 11–15 μm. (**b**) Transmission electron microscopy analysis in wt and IDS-ko cells at stem (0 div) and differentiated (7 div) stage. Scale bars: 6 μm; in inset: 1.7–2.3 μm. (**c**) Quantification of average lysosomal area and diameter (Feret) confirmed the presence of macro-lysosomal organelles in IDS-ko differentiated cells. Values are means ± S.E.M. (**d** and **e**) Western blot analysis (**d**) and enzymatic activity assay (**e**) of IDS in wt cells at 0, 3, 4 and 7 div. The differences among all the values were statistically not significant unless indicated (*$P \leq 0.05$, **$P \leq 0.01$, ***$P \leq 0.001$); Student's *t*-test for all experiments was applied. (**f**) Confocal microscopy images of wt and IDS-ko mouse brain cortex stained against Lamp1. Scale bars: 75 μm. Zoomed images scale bars: 11–15 μm. (**g**) Confocal microscopy images of brain cortex from a healthy and Hunter patient stained against Lamp1. Scale bars: 75 μm; in inset: 17–25 μm. Zoomed images scale bars: 15–31 μm

Lysosome anomalies increase with differentiation. To determine whether GAG accumulation because of IDS deficit could hamper normal differentiation of IDS-ko NSCs, we evaluated lysosomal aggregation as a pathological hallmark correlated with GAG accumulation. We investigated the expression of the lysosomal marker lysosomal-associated membrane protein 1 (Lamp1) both *in vitro* during differentiation and *in vivo*, in the IDS-ko mouse brain and in human Hunter cortex. Although only incipient at the undifferentiated stage (Figure 2a, 0 days *in vitro* (div)), a massive accumulation of Lamp1+ lysosomal organelles was evident after 7 days of differentiation in IDS-ko cells (Figure 2a, 7 div). In particular, the lysosomal accumulation colocalized with glial fibrillary acidic protein+ (GFAP+) astrocytes and galactocerebroside C+ (GalC+) oligodendrocites, and only occasionally with β-tubulin III+ (β-tubIII+) neurons (Figure 2a), suggesting that IDS deficit primarily affects glial cells. Consistently, analysis by transmission electron microscopy showed that undifferentiated IDS-ko NSCs displayed sporadic multivesicular bodies (Figure 2b, 0 div) that were absent in wt NSCs (Figure 2b, 0 div), and these lysosomal anomalies appeared to exacerbate over differentiation (Figure 2b, 7 div). IDS-ko cells displayed massive vacuolization (inset in Figure 2b, 7 div bottom center and right) and aberrant autophagosome-like vesicles (inset in Figure 2b, bottom right), whereas wt cells maintained a normal pattern (Figure 2b, upper center). Average lysosomal area in IDS-ko differentiated cells was $1.07\,\mu m^2 \pm 0.40$ *versus* $0.30\,\mu m^2 \pm 0.10$ in wt cells ($P \leq 0.05$), with, respectively, a maximal Feret diameter of $0.91\,\mu m \pm 0.11$ *versus* $0.59\,\mu m \pm 0.05$ (Figure 2c). We next investigated how IDS expression is normally regulated during differentiation. IDS protein level (Figure 2d) in wt NSCs correlated with enzymatic activity (Figure 2e) and peaked at 3 div, a checkpoint when most NSCs are committed progenitors, and decreased with terminal differentiation. This suggests that IDS deficit induces precocious differentiation of NSCs conditioning long-term survival of transient progenitors. We then analyzed the *in vivo* samples. In wt animals, lysosomes were homogeneously distributed throughout the brain and no aberrant accumulation was detectable (Figure 2f). Consistent with the *in vitro* results, lysosomal aggregation appeared incipient in glial cells of IDS-ko mouse brains at an early symptomatic stage (p42; Supplementary Figure 3). At symptomatic stage (8 months), Lamp1+ lysosomal aggregates were particularly evident in mature brain areas such as cortex (Figure 2f), striatum, septum and olfactory bulbs (OBs), while less evident in the stem niche of the SVZ (Supplementary Figure 2) and mostly colocalizing with GFAP+ astroglial cells and myelin basic protein+ (MBP+) myelin fibers (Figure 2f, zoomed images). No β-tubIII+ cells displayed abnormal lysosomal patterns (Figure 2f, zoomed image) until the end stage (11 months; Supplementary Figure 3). Interestingly, an analogous pattern was observed in the brain cortex of a Hunter patient (Figure 2g). In the healthy human brain (Figure 2g, healthy), only sporadic cells with evident lysosomal aggregation could be detected. In these cells, Lamp1+ organelles displayed a chain-like morphology (Figure 2g, inset in healthy), whereas in the Hunter brain they appeared clustered and distributed throughout the cytosol (Figure 2f, inset in Hunter). These findings suggest IDS-ko NSCs as a valid tool to mimic MPSII pathology and glial degeneration as possibly preceding and contributing to later neuronal death.

Pathological differentiation and apoptosis of IDS-ko NSCs is cell-density dependent. Previous studies on neural progenitor cells from MPSVII mice showed that GAG accumulation because of β-glucuronidase deficiency does not alter neuronal differentiation.[18] To assess whether lysosomal accumulation in IDS-ko glial cells could alter neuronal and/or glial differentiation or maturation, we investigated the differentiation potential of wt and IDS-ko NSCs. We first analyzed the expression of the stem-related marker nestin. The reduction of nestin+ cells during differentiation appeared accelerated in IDS-ko cells with respect to wt (Supplementary Figures 3A and B): at 0 div, IDS-ko and wt neurospheres contained comparable percentages of nestin+ NSCs, whereas at 7 div the number was significantly lower in IDS-ko cells (Supplementary Figure 3B).

We then evaluated the expression of later neuronal and glial markers: β-tubIII and microtubule-associated protein 2 (MAP2) in neurons, GalC in oligodendrocytes and GFAP in astrocytes. In accordance with the rapid decrease of nestin+ cells, we observed that, at 0 div, IDS-ko NSCs displayed a precocious expression of neuronal and oligodendroglial markers (Supplementary Figures S3C–G,I,J). Moreover, at 7 div, a higher percentage of β-tubIII+ neuronal cells and of

Figure 3 Effect of cell density over IDS-ko NSCs differentiation. (**a–f**) Coimmunostaining for caspase3+ and ubiquitin with the neural differentiation markers β-tubIII, GFAP and GalC of wt and IDS-ko NSCs at 0 and 17 div of differentiation under HD (1.25×10^4 cells/cm^2) and LD (6.5×10^3 cells/cm^2) cell density conditions. (**a**) Confocal microscopy images showing the coimmunostaining of caspase3 marker with GFAP, GalC or β-tubIII under HD or low LD conditions. Scale bar: 100 μm. (**b**) Quantification of GFAP+, β-tubIII+ and GalC+ cells over total DAPI+ nuclei under HD and LD conditions. (**c**) Quantification of caspase3+ cells over total DAPI+ nuclei under HD and LD conditions. (**d**) Quantification of GFAP+/caspase3+, β-tubIII/caspase3+, GalC+/caspase3+ cells over total caspase3+ cells under HD and LD conditions. (**e**) Confocal microscopy images showing the immunostaining of ubiquitin+ marker. Scale bar: 100 μm. (**f**) Quantification of ubiquitin+ cells over total DAPI+ nuclei under HD and LD conditions. (**g**) Confocal microscopy images showing the presence of caspase3+ cells in wt (upper left) and IDS-ko (upper right) mouse cortex. Scale bar: 75 μm; in inset: 11.72 μm. Quantification of caspase3+ cells over total DAPI+ nuclei (bottom left) and colocalization with glial markers GFAP (bottom center) and MBP (bottom right). Scale bars: 21, 10 μm. (**h**) Confocal microscopy images showing the presence of ubiquitin+ cells in wt (upper left) and IDS-ko (upper right) mouse cortex. Scale bar: 75 μm. Inset scale bar: 16 μm. Quantification of ubiquitin+ cells over total DAPI+ nuclei (bottom left) and colocalization with GFAP (bottom center) and MBP (bottom right). Scale bar: 13.7 μm. (**i**) Confocal microscopy images showing the presence of caspase3+ cells in wt (upper left) and Hunter (upper right) human cortex (end stage). Scale bar: 75 μm. Quantification of caspase3+ cells over total DAPI+ nuclei (bottom left) and colocalization with GFAP (bottom center), MBP (bottom right) and neuronal marker β-tubIII (bottom right). Scale bar: 10–14 μm. (**j**) Confocal microscopy images showing the presence of ubiquitin+ aggregates in wt (upper left) and Hunter (upper right) human cortex (end stage). Scale bar: 75 μm. Quantification of caspase3+ cells over total DAPI+ nuclei (bottom left) and colocalization with GFAP (bottom center), MBP (bottom right) and β-tubIII (bottom right). Scale bars: 16–18 μm. Student's *t*-test was applied, the differences among all the values were statistically not significant unless indicated (*$P \leq 0.05$,**$P \leq 0.01$, ***$P \leq 0.001$) values are means ± S.E.M. Casp, active caspase 3; Ub, ubiquitin

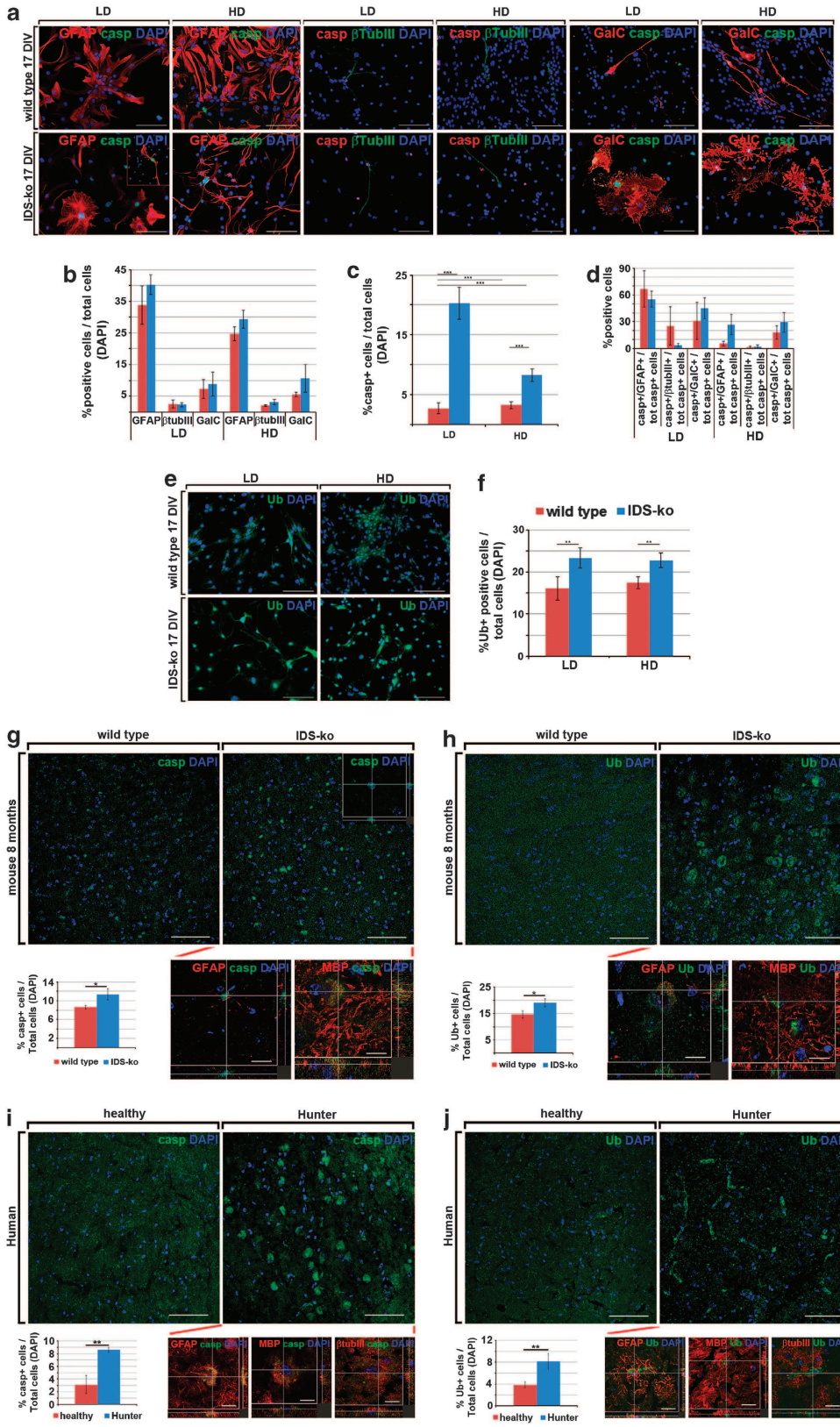
a
LD
HD
wild type 17 DIV
IDS-ko 17 DIV
GFAP casp DAPI
casp βTubIII DAPI
GalC casp DAPI
b
%positive cells / total cells (DAPI)
GFAP
βtubIII
GalC
c
%casp+ cells / total cells (DAPI)
d
%positive cells
e
Ub DAPI
f
wild type
IDS-ko
%Ub+ positive cells / total cells (DAPI)
g
mouse 8 months
casp DAPI
GFAP casp DAPI
MBP casp DAPI
% casp+ cells / Total cells (DAPI)
h
Ub DAPI
GFAP Ub DAPI
MBP Ub DAPI
% Ub+ cells / Total cells (DAPI)
i
Human
healthy
Hunter
βtubIII casp DAPI
j
βtubIII Ub DAPI

GalC + oligodendrocytes was present in IDS-ko NSC-derived progeny compared with wt control (Supplementary Figures 3C, D, I and J), with a decrease of GFAP + cells (Supplementary Figures 3C and D). The morphology of IDS-ko cells also appeared more differentiated with respect to the wt counterparts (Supplementary Figures 3C, F and I), with evidence of emerging processes at 0 div (Supplementary Figures 3C, F and I, white arrows) becoming long and branching at 7 div.

These observations suggest that IDS-ko NSCs retain multipotency, but display an inherent bias to precocious differentiation and/or maturation, leading to suppose that

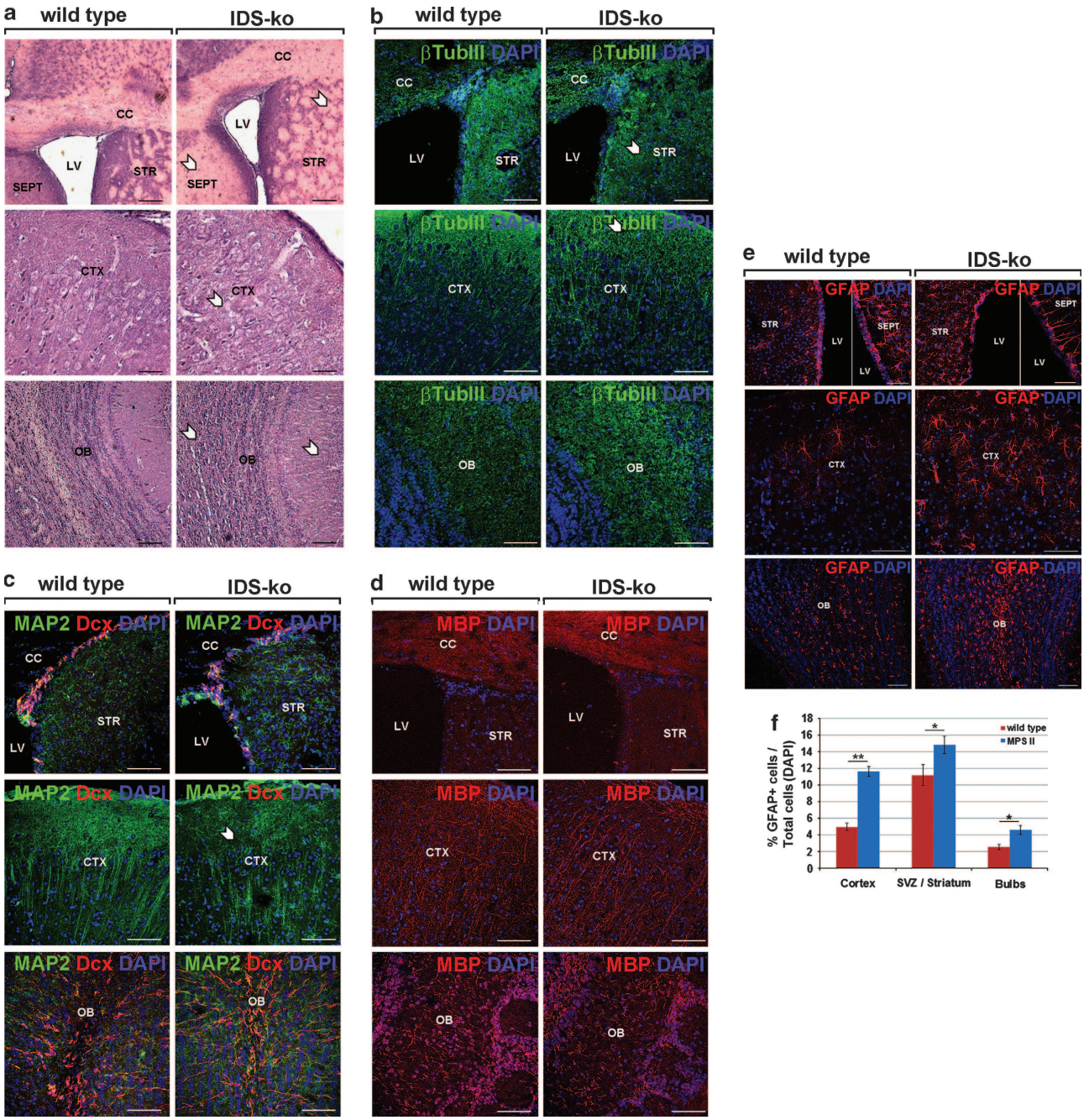

Figure 4 Neurogenic pattern of IDS-ko mouse brain. (**a**) Hematoxylin–eosin histochemical staining of wt and IDS-ko mouse brains. Scale bar in top and bottom pictures: 100 μm; scale bar in center pictures (cortex): 50 μm. (**b–d**) Confocal microscopy images of SVZ, cc, CTX and OB immunostained with antibodies against the neural markers β-tubIII (**b**), MAP2 (**c**), Dcx (**c**) and MBP (**d**). A disorganization of β-tubIII +, MAP2 + and MBP + cells is particularly pronounced in cortex (white arrows). Scale bars: 75 μm. (**e**) Confocal microscopy images of wt and IDS-ko mouse brain immunostained for the astroglial GFAP (**e**) marker. The morphology of GFAP + cells is radial glia-like in IDS-ko SVZ (upper right), whereas star-shaped in wt SVZ (upper left). Scale bars: 75–100 μm; in insets: 10–12 μm. (**f**) Quantification of GFAP + cells over total DAPI + nuclei confirms a remarkable astrogliosis in all the brain areas analyzed. Student's *t*-test was applied, values are means ± S.E.M. cc, corpus callosum; SEPT, septum; CTX, cortex; OB, olfactory bulbs; SVZ, subventricular zone

GAG accumulation deriving from IDS deficit could lead to an accelerated neurogenetic process *in vivo* and ensuing precocious apoptosis of neural cells. To test this hypothesis *in vitro*, we forced long-term differentiation under low cell density (LD) conditions (6.5×10^3cells/cm^2). At 17 div, IDS-ko cells spontaneously originated a lower number of oligodendrocytes with respect to cells cultured under high cell density (HD) conditions (2.5×10^4cells/cm^2) (Figures 3a and b). We next investigated the number of active caspase3+ cells to assess whether IDS-ko differentiated cells undergo precocious apoptosis. At 17 div, under HD, a significantly higher percentage of IDS-ko differentiated cells was caspase3+ ($8.21 \pm 1.03\%$) with respect to wt cells ($3.19 \pm 0.53\%$, $P \leq 0.001$) (Figure 3c). This effect appeared further enhanced at LD, where the number of mutant apoptotic cells raised to $20.26 \pm 2.72\%$ compared with $2.65 \pm 0.87\%$ ($P \leq 0.001$) of wt apoptotic cells (Figure 3c). Interestingly, under both HD and LD, most of caspase3+ cells were GFAP+ astrocytes and GalC+ oligodendrocytes in IDS-ko cells (Figure 3d).

Similar results were obtained by the analysis of ubiquitin aggregates, which are associated to apoptosis-related catabolism of degradation products.[19] Unlike wt cells, mutant cells displayed a heterogeneous distribution of ubiquitin, which appeared concentrated in the perinuclear area and showed irregular protein aggregates under HD and LD (Figures 3e and f).

To correlate the *in vitro* analysis with the pathology in the animal model, we investigated the number of caspase3+ cells and the presence of ubiquitin aggregates *in vivo*. In the IDS-ko mouse, we found an incipient lysosomal aggregates at early symtomatic stage (Supplementary Figure 4) and a significantly higher percentage of caspase3+ cells and of ubiquitin+ aggregates with respect to wt in the cortex and striatum at symptomatic stage (Figures 3g and h). On the contrary, no remarkable differences were detectable in the SVZ of mutant and wt animals (Supplementary Figure 4A). Importantly, caspase3+ cells and ubiquitin aggregates mostly colocalized with GFAP (zoomed images in Figure 3g) or MBP (zoomed images in Figure 3h) glial markers, whereas not with the neuronal marker β-tubIII+. The presence of neuronal apoptotic cells was evident only at later stages (Supplementary Figure 4B),[20] suggesting that degeneration of glial cells precedes that of neuronal cells in an age-dependent manner.

The results obtained were consistent with those from the analysis of the Hunter patient (Figures 3i and j). The fraction of caspase3+ and of ubiquitin+ cells in the Hunter cortex was higher ($P \leq 0.01$) than in the wt brain (Figures 3i and j). GFAP+, MBP+ and β-tubIII+ cells were identified as colabeled with caspase3 (zoomed images in Figure3i) or ubiquitin (zoomed images in Figure3j) antibodies, confirming the presence of both glial and neuronal degeneration at the terminal point (death) of disease progression in humans. On the contrary, no differences were observed between healthy and Hunter SVZs. Although we cannot exclude that other regulatory processes independent of NSC biology, such as neuroinflammation, may be responsible for the observed neurodegeneration, these results suggest an important involvement of glial cells in MPSII pathology.

IDS deficit affects mature brain areas. We next sought to determine to what extent the neurogenic pattern is hampered in IDS-ko mouse brain. A preliminary hematoxylin-eosin histochemical analysis revealed loose and disorganized tissue architecture in the striatum, septum, corpus callosum, cortex and OBs of IDS-ko mice (Figure 4a). Unlike the regular and homogeneous distribution of neuronal cells in the mature brain areas of wt animals, both β-tubIII+ (Figure 4b) and MAP2+ (Figure 4c) neuronal cells were chaotically intermingled in IDS-ko mouse brains, although the number of NeuN+ cells remained unaltered (not shown). To exclude that a lower number of early neuronal progenitor cells could account for the poor neurogenesis, we investigated the expression of double cortin (Dcx), a neuronal progenitor marker. Although only sporadically detectable in cortex and striatum, Dcx+ cells appeared numerous in the OBs and in the SVZ of IDS-ko brains (Figure 4c), but their number and morphology did not appear significantly different from wt. Indeed, the SVZ regions of IDS-ko and wt mice appeared indistinguishable (Supplementary Figure 2), supporting the hypothesis that GAG metabolism has no significant influence on NSC self-renewal or early differentiation neither *in vitro* nor *in vivo*. When analyzing the myelin pattern, MBP+ cells in IDS-ko mice displayed a disorganization complementary to that of neuronal cells (Figure 4d), but no evident reduction of MBP was detectable by densitometric analysis. On the contrary, we observed a remarkable increase of activated GFAP+ cells in the IDS-ko brain (Figures 4e and f).

A similar patterning was observed in the human cortex from an end-stage Hunter patient (Supplementary Figure 5).

IDS deficit induces degeneration of platelet-derived growth factor receptor-α-positive (PDGFRα+) progenitors. After observing that astroglial GFAP+ cells were more numerous and morphologically reactive in IDS-ko *versus* wt brains (Figures 4e and f), we investigated the number and distribution of PDGFRα+ neural progenitors, which appeared reduced and with a remarkably altered morphology in the brain of mutant mice (Figure 5b). Although normal PDGFRα+ cells presented a small cell body with long processes, mutant cells appeared fibrotic and amoeboid with short branching (Figure 5a). To exclude that this could depend on defective neurogenesis from the SVZ, we counted the number of PDGFRα+ cells in the SVZ of mutant and wt mice and detected no differences. Interestingly, a very similar pattern was present in the cortex of the Hunter patient (Figure 5c), where the number of PDGFRα+ cells was reduced with respect to the control (Figure 5d), whereas the healthy and Hunter SVZs appeared undistinguishable. Following these observations, we translated the analysis to the IDS-ko NSCs. When PDGF was added to the culture medium to potentiate the proliferation of PDGFRα+ cells,[21] mutant neurospheres showed a more modest growth rate enhancement than wt NSCs (Figure 5e). This divergence appeared further enhanced after removal of EGF, a condition that privileges the expansion of PDGFRα-responsive cells (Figure 5f). Effects obtained from PDGF treatment were compared with the addition of recombinant IDS from expansion throughout differentiation. Enzyme activity assay confirmed that the IDS enzyme was taken up by mutant cells

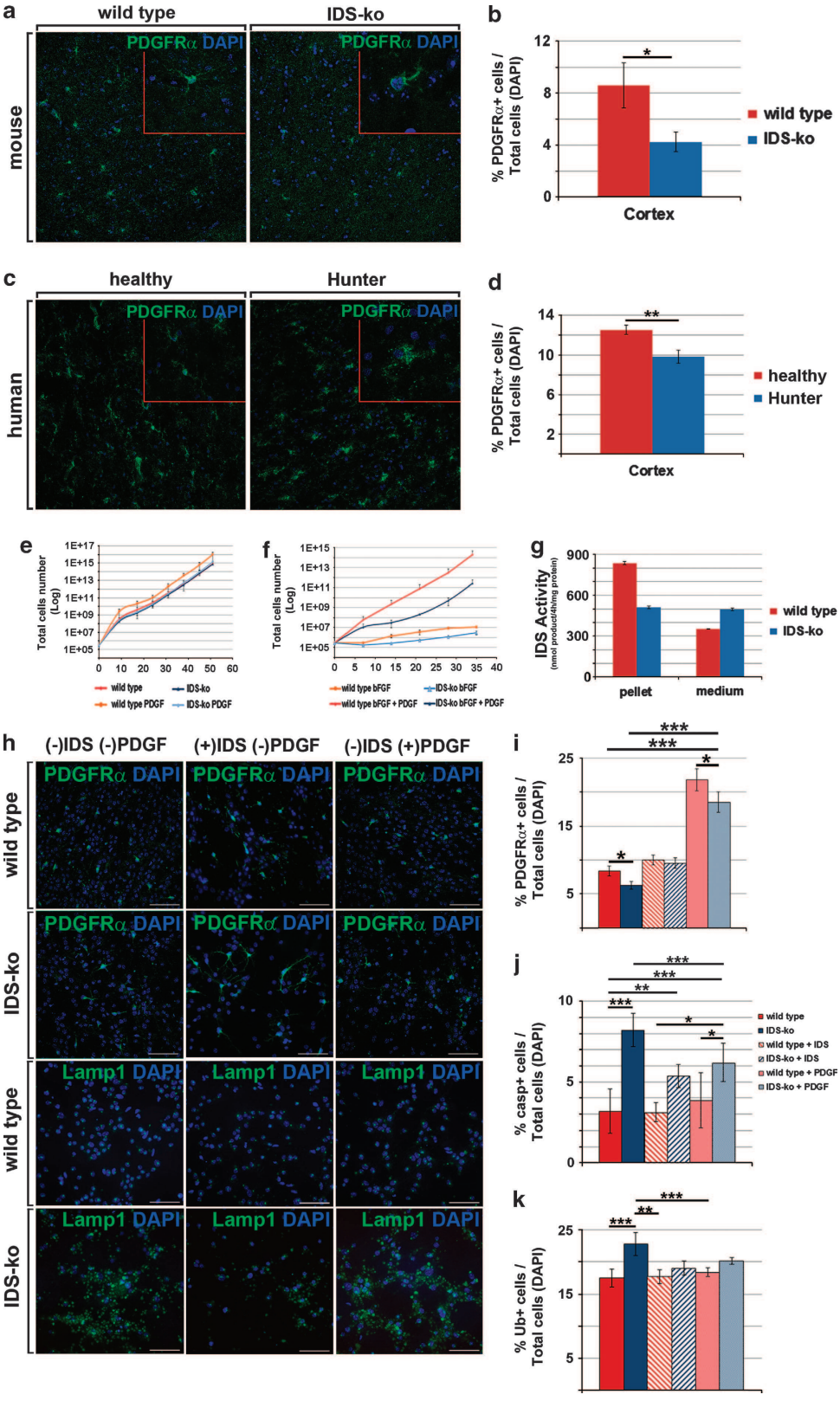
a
wild type
IDS-ko
mouse
PDGFRα DAPI
b
% PDGFRα+ cells / Total cells (DAPI)
Cortex
wild type
IDS-ko
c
healthy
Hunter
human
d
healthy
Hunter
e
Total cells number (Log)
wild type
IDS-ko
wild type PDGF
IDS-ko PDGF
f
wild type bFGF
IDS-ko bFGF
wild type bFGF + PDGF
IDS-ko bFGF + PDGF
g
IDS Activity
pellet
medium
h
(-)IDS (-)PDGF
(+)IDS (-)PDGF
(-)IDS (+)PDGF
Lamp1 DAPI
i
j
% casp+ cells / Total cells (DAPI)
wild type + IDS
IDS-ko + IDS
wild type + PDGF
IDS-ko + PDGF
k
% Ub+ cells / Total cells (DAPI)

and was functionally active (Figure 5g). We observed an increase of PDGFR$\alpha+$ progenitors and a reduction of Lamp1$+$ aggregates in IDS-treated IDS-ko NSCs and to a lesser extent after PDGF treatment (Figure 5h). We evaluated the number of PDGFR$\alpha+$, caspase3$+$ and ubiquitin$+$ cells in untreated, IDS- and PDGF-treated cells after 17 div (Figures 5i–k). Interestingly, the fraction of PDGFR$\alpha+$ cells was remarkably increased in MPSII cultures treated with either IDS or PDGF with respect to untreated controls (Figure 5i). In wt cells, a similar increase of PDGFR$\alpha+$ cells was obtained by treatment with PDGF, whereas no significant differences were evident between untreated and IDS-treated cells (Figure 5i).

In accordance with the partial rescue of PDGFR$\alpha+$ cells, the number of caspase3$+$ apoptotic cells in IDS-ko NSC-derived progeny was significantly decreased by both IDS and PDGF treatments compared with untreated cells (Figure 5j).

Similarly, the percentage of mutant cells displaying ubiquitin aggregates was dampened by IDS treatment (Figure 5k), whereas PDGF treatment did not induce significant effects (Figure 5k).

These results suggest the involvement of PDGF signaling in MPSII pathogenesis and that treatment with PDGF could contribute to ameliorate the pathological environment, although it does not suffice for the complete rescue of the pathology.

Discussion

With the aim to recapitulate the pipeline of MPSII neuropathology, we analyzed the differentiation pattern of NSCs derived from the SVZ of early symptomatic IDS-ko mice in comparison with a time-course analysis of MPSII mouse brains at different stages of the disease and with a human Hunter cortex. Consistent with previous studies,[18] mutant NSCs displayed a self-renewal capacity comparable to wt NSCs, suggesting that IDS activity is not crucial for stem cell metabolism or to maintain a stable self-renewal. However, their dependence on the removal of mitogens from the culture medium was initially remarkably higher, suggesting that IDS deficit could hamper normal differentiation. Indeed, during differentiation, IDS-ko NSCs displayed an increasing and robust accumulation of lysosomal organelles, which was absent in normal cells. Interestingly, both IDS expression and activity in normal cells peaked at the progenitor stage leading to speculate that IDS could prime the correct commitment of transient progenitors and/or contribute to establish an extracellular environment suitable to functional differentiation and survival of mature cells.

Consistently, the precocious expression of neuronal and glial markers in mutant NSCs was accompanied by the rapid achievement of a specialized morphology and followed by an increase of apoptotic cells, suggesting a quicker differentiation of IDS-ko NSC, which was enhanced by stringent culture conditions (LD). In particular, most lysosomal aggregates were detected in glial cells *in vitro* and a comparable patterning could be observed in IDS-ko mouse brains, suggesting that late neuronal degeneration *in vivo* (11 months aged IDS-ko mouse brain and human Hunter's brain)[20] could depend on a primary degeneration of non-neuronal cells. It must be considered that various mechanisms are involved in LSD pathogenesis.[22] Accumulation in the extracellular matrix (ECM) of heparan- and dermatan-sulfate fragments with altered sulphation pattern could affect signal transduction pathways, as previously described in MPSI.[23] This could hinder the development of appropriate cell–cell contacts between neuronal and oligodendroglial or astroglial cells, which have a key role in driving correct neurogenetic processes. In accordance with this hypothesis, we observed that under LD conditions, precocious differentiation and apoptosis of IDS-ko NSC-derived progeny were enhanced. Indeed, Lemonnier *et al.*[15] recently demonstrated that gene expression profiling in NSCs derived from MPSIIIB induced pluripotent stem cells (iPSCs) shows dramatic alterations of ECM components and of cell–matrix interactions. In this view, we cannot exclude that early cell apoptosis could depend on other reasons aside from developmental programming and the analysis of ECM in Hunter's brain would deserve further attention in future studies.

In parallel with *in vitro* studies, we investigated the integrity of the neural tissue and performed a detailed characterization of the IDS-ko mouse brain. Many lysosomal and ubiquitin aggregates were present in the IDS-ko brain parenchyma together with a disorganized cytoarchitecture and a significant number of apoptotic cells, mostly GFAP$+$ astrocytes and MBP$+$ oligodendrocytes, supporting our hypothesis that neuronal degeneration follows glial cell death.[20] This pattern was consistent with the evidence from IDS-ko NSC differentiation *in vitro* and, importantly, mirrored that of the brain cortex of an end-stage MPSII patient, except for the fact that the human cortex displayed the presence of both glial and neuronal apoptotic cells, similar to the pattern of end-stage IDS-ko mice.[20] The lack of human samples hampered the analysis at earlier stages of the disease, but our observation is

Figure 5 IDS deficiency affects the number of PDGFR-$\alpha+$ progenitors both in mouse and in human: potential therapeutic effects of PDGF. (**a**) Confocal microscopy images of wt and IDS-ko mice brain cortex immunostained for the glial PDGFRα marker. Scale bar: 75 μm. Inset images show the difference between the wt long-branching and the mutant round-shaped morphologies of PDGFR$\alpha+$ cells. Scale bars: 26 μm in wt and 8 μm in IDS-ko. (**b**) Quantification of PDGFR$\alpha+$ cells over total DAPI$+$ cells. (**c**) Confocal microscopy images of wt and Hunter human cortex immunostained for the glial PDGFRα marker. Scale bar: 75 μm. Inset images show the difference between the wt long-branching and the mutant disrupted morphologies of PDGFR$\alpha+$ cells. Scale bars: 22 μm in healthy and 11 μm in Hunter. (**d**) Quantification of PDGFR$\alpha+$ cells over total DAPI$+$ cells. (**e** and **f**) Graphs showing the proliferation rate of wt NSC (red, orange) and IDS-ko NSC (blue, light blue) when cultured in the presence of both EGF and FGF2 (E) or FGF2 alone (**f**) with or without addition of PDGF. (**g**) Enzymatic IDS activity assay in wt and IDS-ko murine NSCs and related supernatants after addition of IDS to the culture medium for 5 div, showing the rescue of IDS activity in IDS-ko cells. (**h**) Confocal microscopy images of wt and IDS-ko NSCs cultured and differentiated for 10 div with or without addition of IDS or PDGF to the culture media and immunostained with antibodies against PDGFRα and Lamp1. (**i–k**) Histograms showing the percentage of PDGFR$\alpha+$ (**i**), Caspase 3$+$ (**j**) and ubiquitin$+$ (**k**) cells over total nuclei in untreated, PDGF- or IDS-treated wt and IDS-ko NSCs differentiated for 10 div.The differences among all the values were statistically not significant unless indicated (*$P\leq0.05$, **$P\leq0.01$, ***$P\leq0.001$); Student's *t*-test was applied for **b**, **d** and **g**, whereas one-way ANOVA followed by Student's *t*-test for **i**, **j** and **k** experiments

consistent with late neuronal damage driven by glial degeneration. Hence, although not further explored and beyond the aim of this study, epigenetic modifications could be assumed to have a role in MPSII, and will be addressed in future studies to elucidate the involvement of specific proteins or molecules such as neurotrophic factors, ECM components and chemoattractants.[24,25]

In this view, the use of NSCs derived from IDS-ko mice for modeling MPSII pathogenesis holds great promise, although it is not flawless: a number of mechanisms which underpin MPSII pathogenesis are likely related to the central nervous system microenvironment and non-neural cell-mediated and may not be recapitulated by NSC modeling *in vitro*, such as chronic inflammation.[22] In the same areas with major lysosomal aggregation and tissue disorganization, we found a dramatic increase of fibroblast-like astrocytes, entailing that astrogliosis was concomitant with an evolving inflammatory environment.

A recent study[26] showed that two distinct subsets of progenitors coexist in the SVZ: GFAP-expressing NCSs and PDGFRα-expressing progenitors. In our study, conversely to GFAP+ cells, we observed a defective pool of PDGFR-α+ progenitors in the cortex of IDS-ko mouse brain and of the human Hunter patient. Whether the defective pool of PDGFR-α+ neural progenitors is due to a deficient generation from NSCs in the SVZ, to a dysregulation of the PDGF/PDGFR autocrine loop[21] or to other secondary pleiotropic effects during neurogenesis, has still to be definitely shown. As no alterations were evident in the SVZ, our data tend to exclude the first hypothesis. However, these observed changes also occurred *in vitro* in our model system. Mutant NSCs generated a lower fraction of PDGFR-α progenitors *in vitro* than wt cells and this impairment was reverted by IDS treatment, similar to what ERT does *in vivo*, thus supporting NSCs as a tool to model MPSII *ex vivo*. Moreover, the addition of PDGF to IDS-ko NSCs partially mimicked the effects of the IDS enzyme suggesting PDGF, already known to bind GAGs and differentially regulate their mitogenic function,[27,28] as involved in the survival of neural progenitors in a LSD disease.

Unlike recent evidence of defective self-renewal of iPSCs from MPSVII patients,[29] in our study IDS deficit appears not to affect NSC proliferation, thus entailing that brain development during the embryonic stage may be normal. The characterization of the IDS-ko adult mouse brain and the unique parallelism with the analysis of a human Hunter brain strengthen our findings, emphasizing their clinical relevance and the reliability of the IDS-ko animal model for neuropathogenetic evaluations.

This is the first report suggesting abnormal NSC-derived glial progenitor differentiation as a potential mechanism for the development of MPSII neuropathology and we were able to modulate the mutant phenotype of IDS-ko NSCs *in vitro* by ERT or PDGF treatment, thus fostering NSCs as a valid tool for drug screening and PDGF as a candidate molecule for a combined therapeutic approach to MPSII. On the basis of our results, we propose the transplantation of NSC-derived glial progenitors, or the injection of PDGF and other gliotrophins combined with ERT, among the strategies for future clinical applications.[30]

Materials and Methods

Mice. C57BL6 IDS-ko mice were kindly provided by J Muenzer (University of North Carolina, NC, USA), C57BL6 wt mice were purchased from Harlan Italy (Milano, Italy). ko and wt mice were housed in light- and temperature-controlled conditions, with food and water provided *ad libitum*. All animal care and experimental procedures were conducted according to the current national and international animal ethics guidelines.

Human specimen. Human tissue was obtained from the NIHCD Brain and Tissue Bank for Developmental Disorders at the University of Maryland, Baltimore, MD, USA (UMB#M1987 for Hunter's sample; UMB#5387 for the age-matched healthy control).

Propagation and differentiation of mouse NSCs. Two wt and two IDS-ko neural stem cell lines were isolated and propagated from the SVZ of adult mouse brains at 6–7 weeks of age as described by Vescovi *et al.*[31] Here all results will be presented as the average of the two IDS-ko and of the two wt NSC lines, respectively.

Differentiation of NSCs. To induce NSC differentiation, individual spheres were mechanically dissociated and cells were transferred at 2.5×10^4cells/cm^2 high-density conditions) or 6.5×10^3cells/cm^2 (low-density conditions) onto cultrex-coated chamber-slides and differentiated as described in Gritti *et al.*[32] for a total of 7 or 17 days. Where indicated, cells were treated throughout differentiation with PDGF (20 ng/ml; Peprotech, Rocky Hill, NJ, USA) or IDS enzyme (4 μg/ml). Human recombinant IDS was obtained as a pool of residual microvolumes following patients administration.

Generation of growth curves. The rate of expansion of the NSCs was obtained by plating 3×10^5cells in separate T25 flasks in growth medium containing FGF2 (20 ng/ml) and EGF (10 ng/ml; Peprotech) and PDGF (20 ng/ml; Peprotech) in different combinations where indicated. At each passage (p), NSC-originated neurospheres were dissociated the total cell number was calculated on the basis of amplification rate at each passage; the logarithmic value of the total viable-cell number was plotted against the div, starting from the beginning of the experiment. For each condition, growth curves were performed in duplicate.

Immunocytochemistry. Cultures were fixed in freshly prepared, buffered 4% paraformaldehyde. After blocking with 10% normal goat serum, cultures were incubated overnight at 4 °C with the following antibodies (monoclonal antibody, monoclonal; polyclonal antibody, polyclonal): nestin (monoclonal, MAB 353, Millipore, Bedford, MA, USA; 1:200, Species Cross Reactivity: mouse, rat), β-tubIII (monoclonal, MMS-435P, Covance, Princeton, NJ, USA; 1:400, Species Cross Reactivity: mammalian), GFAP (polyclonal, Dako, Glostrup, Denmark; 1:400, Species Cross Reactivity: mammalian), GalC (monoclonal, MAB345, Chemicon - Millipore Bioscience Research Reagents, Temecula, CA, USA; 1:100, Species Cross Reactivity: bovine, human, mouse, rat, rabbit), Lamp1 (polyclonal, ab24170, Abcam, Cambridge, UK; 1:750, Species Cross Reactivity: dog, human, mouse, rat, Zebrafish), caspase3 (Asp 170) (polyclonal, #9961, Cell Signaling, Danvers, MA, USA; 1:500, Species Cross Reactivity: human, mouse, rat, monkey, bovine), ubiquitin (polyclonal, Z0458, Dako, 1:50, Species Cross Reactivity: human, mouse, rat), MAP2 (monoclonal, Chemicon, 1:400, Species Cross Reactivity: human, rat, mouse, bovine, chicken), KI67 nuclear antigen (polyclonal, Novocastra - Leica Microsystems GmbH, Wetzlar, Germany; NCL-Ki67p, 1:1000, Species Cross Reactivity: human, mouse), PDGFRα (PDGFRα, polyclonal, #3164, Cell Signaling, 1:100, Species Cross Reactivity: human, mouse, rat).

After removal of the primary antibodies and repeated washes with PBS, cultures were incubated at room temperature (20 °C) for 45 min with secondary antibodies labeled with Alexa Fluor 594or 488 (anti-mouse and/or anti rat, Molecular Probes - Life Technologies, Carlsbad, CA, USA). Samples were then colored with 4′,6-diamidino-2-phenylindole dihydrochloride (DAPI; 0.3 μg/ml, Roche Applied Science, Penzberg, Germany) for nuclear staining and rinsed with PBS for mounting and analysis. Microphotographs were taken using a Zeiss Axiovert 200 direct epifluorescence microscope (Axioplan 2; Carl Zeiss, Jena, Germany) or by confocal microscopy (Leica DM IRE2).

Immunohistochemistry. Mice (6 weeks, 8 and 11 months of age) were euthanized with Avertin (300 mg/kg) and transcardially perfused-fixed with 4% paraformaldehyde. Brains were post-fixed overnight, cryoprotected, frozen and

coronally sectioned (20 μm thick) by cryostat. For the human specimen, sections (20 μm thick) were obtained by cryostat, post-fixed with 4% paraformaldehyde and processed as murine samples. Sections were blocked with 10% normal goat serum and 1% Triton X-100 for 90 min and incubated overnight with the following primary antibodies: GFAP, βtubIII, MAP2, Lamp1, caspase3, ubiquitin, PDGFRα (see immunocytochemistry analysis for dilution), MBP (monoclonal, SMI 99P, Covance, 1:200, Species Cross Reactivity: mammalian), Dcx (C-18) (polyclonal, sc-8066, Santa Cruz Biotechnology, Dallas, TX, USA; 1:200, Species Cross Reactivity: mouse, rat). The fluorescent secondary antibodies used were labeled with Alexa Fluor 549 or 488 (Molecular Probes). DAPI (see immunocytochemistry analysis) was used as nuclear marker. Labeled samples were analyzed by fluorescence microscopy and by confocal microscopy (see immunocytochemistry analysis). Densitometric analysis of human specimen was performed by evaluation of confocal microscopy images ($n = 21$ cells, randomly chosen over $n = 7$ slices per sample) with Laser Pix Software (Bio-Rad Laboratories, Hercules, CA, USA).

Image quantification and statistical analysis. For immunocytochemistry, data are reported as percentages of labeled cells over the total number of nuclei ± S.E.M. An average total amount of 3×10^3 cells (identified by DAPI nuclear staining) was counted randomly from two coverslips per condition in each experiment. Each value represents the average of three independent experiments.

For immunohistochemistry, quantification of the percentage of GFAP+ cells over total DAPI was performed in three regions of interest per section (cortex, subventricular zone (each 200 μm apart) spanning the central region of bregma 0 and adjacent striatum area, OBs). Each value represents the average of $n = 3$ animals unless differently stated in the text.

Statistical analysis was performed by *t*-test and two-ways ANOVA (Bonferroni test). Data are reported as mean ± S.E.M. Data are considered not statistically significant unless indicated in the figures (* indicates $P \leq 0.05$, ** indicates $P \leq 0.01$, *** indicates $P \leq 0.001$).

Western blot analysis. Immunoblots were performed as described.[33] Polyvinylidene fluoride membranes (Millipore) were incubated with rat antibodies against IDS and Notch1 (100-401-407, Rockland) and monoclonal antibodies for glyceraldehyde 3-phosphate dehydrogenase (Sigma-Aldrich, St. Louis, MO, USA), the latter to normalize bands for equal loading of proteins per lane. Bands were quantified by densitometric analysis of the ECL-exposed films.

Electron Microscopy analysis. For standard EM, cell monolayers were washed with phosphate buffer 0.12 M, fixed with 2% glutaraldehyde/4% paraformaldehyde in 0.12 M phosphate buffer (30 min, 20 °C) and post-fixed with 2% OsO_4 in 0.1 M sodium cacodylate buffer. After dehydration in ethanol and overnight infiltration (75% Epon-812, 25% ethanol), samples were embedded in Epon. Ultrathin sections (60 nm thickness) were doubly stained with uranyl acetate and lead citrate and examined with a Philips CM10microscope (Philips, Eindhoven, Netherlands)). Electronic micrographs were captured with a slow scan CCD camera (S.I.S. Megaview III). Lysosomes were measured with Image J software 1.5.0_10 (32 bit).

IDS enzymatic assay. IDS activity was measured by a fluorogenic assay[34] using the artificial substrate 4-methylumbelliferyl-α-L-iduronide-2-sulfate (MU-αIdoA-2S; Moscerdam Substrates, Oegstgeest, Netherlands) according to the manufacturer's instructions. Enzyme activity was given as nmoles of substrate hydrolyzed in 4 h per mg of total protein or per ml of culture medium, using 4-methylumbelliferone (Sigma-Aldrich) as standard. Each value represents the average of three or four independent replicates.

Conflict of Interest

The authors declare no conflict of interest.

Acknowledgements. We thank Anna Villa for densitometric analysis, Alessio Giavazzi, Daniela Ferrari and Manuel Fiorillo for precious support and collaboration. Human tissue was obtained from the NIHCD Brain and Tissue Bank for Developmental Disorders at the University of Maryland, Baltimore, MD, USA. The role of NIHCD Brain and Tissue Bank is to distribute tissue, and therefore, cannot endorse the studies performed or the interpretation of results. The project was funded by Fondazione Cellule Staminali di Terni and partly by the Brains for Brain Foundation (http://www.brains4brain.eu).

1. Muenzer J. Overview of the mucopolysaccharidoses. *Rheumatology (Oxford)* 2011; **50**: v4–v12.
2. Scarpa M, Almassy Z, Beck M, Bodamer O, Bruce IA, De Meirleir L *et al.* Mucopolysaccharidosis type II: European recommendations for the diagnosis and multidisciplinary management of a rare disease. *Orphanet J Rare Dis* 2011; **6**: 72.
3. Muenzer J, Beck M, Eng CM, Giugliani R, Harmatz P, Martin R *et al.* Long-term, open-labeled extension study of idursulfase in the treatment of Hunter syndrome. *Genet Med* 2011; **13**: 95–101.
4. Muenzer J, Beck M, Giugliani R, Suzuki Y, Tylki-Szymanska A, Valayannopoulos V *et al.* Idursulfase treatment of Hunter syndrome in children younger than 6 years: results from the Hunter Outcome Survey. *Genet Med* 2011; **13**: 102–109.
5. Muenzer J, Bodamer O, Burton B, Clarke L, Frenking GS, Giugliani R *et al.* The role of enzyme replacement therapy in severe Hunter syndrome-an expert panel consensus. *Eur J Pediatr* 2012; **171**: 181–188.
6. Higuchi T, Shimizu H, Fukuda T, Kawagoe S, Matsumoto J, Shimada Y *et al.* Enzyme replacement therapy (ERT) procedure for mucopolysaccharidosis type II (MPS II) by intraventricular administration (IVA) in murine MPS II. *Mol Genet Metab* 2012; **107**: 122–128.
7. Polito VA, Abbondante S, Polishchuk RS, Nusco E, Salvia R, Cosma MP. Correction of CNS defects in the MPSII mouse model via systemic enzyme replacement therapy. *Hum Mol Genet* 2010; **19**: 4871–4885.
8. Cardone M, Polito VA, Pepe S, Mann L, D'Azzo A, Auricchio A *et al.* Correction of Hunter syndrome in the MPSII mouse model by AAV2/8-mediated gene delivery. *Hum Mol Genet* 2006; **15**: 1225–1236.
9. Vogler C, Levy B, Grubb JH, Galvin N, Tan Y, Kakkis E *et al.* Overcoming the blood-brain barrier with high-dose enzyme replacement therapy in murine mucopolysaccharidosis VII. *Proc Natl Acad Sci USA* 2005; **102**: 14777–14782.
10. Muenzer J, Gucsavas-Calikoglu M, McCandless SE, Schuetz TJ, Kimura A. A phase I/II clinical trial of enzyme replacement therapy in mucopolysaccharidosis II (Hunter syndrome). *Mol Genet Metab* 2007; **90**: 329–337.
11. Muenzer J, Wraith JE, Beck M, Giugliani R, Harmatz P, Eng CM *et al.* A phase II/III clinical study of enzyme replacement therapy with idursulfase in mucopolysaccharidosis II (Hunter syndrome). *Genet Med* 2006; **8**: 465–473.
12. Wraith JE. Enzyme replacement therapy with idursulfase in patients with mucopolysaccharidosis type II. *Acta Paediatr Suppl* 2008; **97**: 76–78.
13. Tomanin R, Zanetti A, Zaccariotto E, D'Avanzo F, Bellettato CM, Scarpa M. Gene therapy approaches for lysosomal storage disorders, a good model for the treatment of mendelian diseases. *Acta Paediatr* 2012; **101**: 692–701.
14. Givogri MI, Bottai D, Zhu HL, Fasano S, Lamorte G, Brambilla R *et al.* Multipotential neural precursors transplanted into the metachromatic leukodystrophy brain fail to generate oligodendrocytes but contribute to limit brain dysfunction. *Dev Neurosci* 2008; **30**: 340–357.
15. Lemonnier T, Blanchard S, Toli D, Roy E, Bigou S, Froissart R *et al.* Modeling neuronal defects associated with a lysosomal disorder using patient-derived induced pluripotent stem cells. *Hum Mol Genet* 2011; **20**: 3653–3666.
16. Marshall GP 2nd, Reynolds BA, Laywell ED. Using the neurosphere assay to quantify neural stem cells *in vivo*. *Curr Pharm Biotechnol* 2007; **8**: 141–145.
17. Reynolds BA, Rietze RL. Neural stem cells and neurospheres-re-evaluating the relationship. *Nat Methods* 2005; **2**: 333–336.
18. Heuer GG, Skorupa AF, Prasad Alur RK, Jiang K, Wolfe JH. Accumulation of abnormal amounts of glycosaminoglycans in murine mucopolysaccharidosis type VII neural progenitor cells does not alter the growth rate or efficiency of differentiation into neurons. *Mol Cell Neurosci* 2001; **17**: 167–178.
19. Ravikumar B, Sarkar S, Davies JE, Futter M, Garcia-Arencibia M, Green-Thompson ZW *et al.* Regulation of mammalian autophagy in physiology and pathophysiology. *Physiol Rev* 2010; **90**: 1383–1435.
20. Polito VA, Cosma MP. IDS crossing of the blood-brain barrier corrects CNS defects in MPSII mice. *Am J Hum Genet* 2009; **85**: 296–301.
21. Jackson EL, Garcia-Verdugo JM, Gil-Perotin S, Roy M, Quinones-Hinojosa A, VandenBerg S *et al.* PDGFR alpha-positive B cells are neural stem cells in the adult SVZ that form glioma-like growths in response to increased PDGF signaling. *Neuron* 2006; **51**: 187–199.
22. Vitner EB, Platt FM, Futerman AH. Common and uncommon pathogenic cascades in lysosomal storage diseases. *J Biol Chem* 2010; **285**: 20423–20427.
23. Ballabio A, Gieselmann V. Lysosomal disorders: from storage to cellular damage. *Biochim Biophys Acta* 2009; **1793**: 684–696.
24. Decker L, ffrench-Constant C. Lipid rafts and integrin activation regulate oligodendrocyte survival. *J Neurosci* 2004; **24**: 3816–3825.
25. Kazanis I, Lathia JD, Vadakkan TJ, Raborn E, Wan R, Mughal MR *et al.* Quiescence and activation of stem and precursor cell populations in the subependymal zone of the mammalian brain are associated with distinct cellular and extracellular matrix signals. *J Neurosci* 2010; **30**: 9771–9781.
26. Chojnacki A, Mak G, Weiss S. PDGFRalpha expression distinguishes GFAP-expressing neural stem cells from PDGF-responsive neural precursors in the adult periventricular area. *J Neurosci* 2011; **31**: 9503–9512.
27. Fager G, Camejo G, Olsson U, Ostergren-Lunden G, Lustig F, Bondjers G. Binding of platelet-derived growth factor and low density lipoproteins to glycosaminoglycan

species produced by human arterial smooth muscle cells. *J Cell Physiol* 1995; **163**: 380–392.
28. Garcia-Olivas R, Hoebeke J, Castel S, Reina M, Fager G, Lustig F *et al.* Differential binding of platelet-derived growth factor isoforms to glycosaminoglycans. *Histochem Cell Biol* 2003; **120**: 371–382.
29. Meng XL, Shen JS, Kawagoe S, Ohashi T, Brady RO, Eto Y. Induced pluripotent stem cells derived from mouse models of lysosomal storage disorders. *Proc Natl Acad Sci USA* 2010; **107**: 7886–7891.
30. Woodruff RH, Fruttiger M, Richardson WD, Franklin RJ. Platelet-derived growth factor regulates oligodendrocyte progenitor numbers in adult CNS and their response following CNS demyelination. *Mol Cell Neurosci* 2004; **25**: 252–262.
31. Vescovi AL, Reynolds BA, Fraser DD, Weiss S. bFGF regulates the proliferative fate of unipotent (neuronal) and bipotent (neuronal/astroglial) EGF-generated CNS progenitor cells. *Neuron* 1993; **11**: 951–966.
32. Gritti A, Frolichsthal-Schoeller P, Galli R, Parati EA, Cova L, Pagano SF *et al.* Epidermal and fibroblast growth factors behave as mitogenic regulators for a single multipotent stem cell-like population from the subventricular region of the adult mouse forebrain. *J Neurosci* 1999; **19**: 3287–3297.
33. Carlessi L, De Filippis L, Lecis D, Vescovi A, Delia D. DNA-damage response, survival and differentiation in vitro of a human neural stem cell line in relation to ATM expression. *Cell Death Differ* 2009; **16**: 795–806.
34. Voznyi YV, Keulemans JL, van Diggelen OP. A fluorimetric enzyme assay for the diagnosis of MPS II (Hunter disease). *J Inherit Metab Dis* 2001; **24**: 675–680.

Supplementary Information accompanies this paper on Cell Death and Disease website (http://www.nature.com/cddis)